1-1-2017

Design Configurations and Operating Limitations of an Oscillating Heat Pipe

Omar Talal Ibrahim

Design configurations and operating limitations of an oscillating heat pipe

By

Omar Talal Ibrahim

A Dissertation
Submitted to the Faculty of
Mississippi State University
in Partial Fulfillment of the Requirements
for the Degree of Doctor of Philosophy
in Mechanical Engineering
in the Department of Mechanical Engineering

Mississippi State, Mississippi

August 2017

Design configurations and operating limitations of an oscillating heat pipe

By

Omar Talal Ibrahim

Approved:

_____

HeeJin Cho
(Major Professor)

_____

Pedro J. Mago
(Committee Member)

_____

Yucheng Liu
(Committee Member)

_____

Shanti Bhushan
(Committee Member)

_____

Yucheng Liu
(Graduate Coordinator)

_____

Jason M. Keith
Dean
Bagley College of Engineering

Name: Omar Talal Ibrahim

Date of Degree: August 11, 2017

Institution: Mississippi State University

Major Field: Mechanical Engineering

Major Professor: HeeJin Cho

Title of Study: Design configurations and operating limitations of an oscillating heat pipe

Pages in Study 81

Candidate for Degree of Doctor of Philosophy

Passive and compact heat dissipation systems are and will remain vital for the successful operation of modern electronic systems. Oscillating heat pipes (OHPs) have been a part of this research area since their inception due to their ability to passively manage high heat fluxes. In the current investigation, different designs of tubular, flat plate, and multiple layer oscillating heat pipes are studied by using different operating parameters to investigate the operating limitations of each design. Furthermore, selective laser melting was demonstrated as a new OHP manufacturing technique and was used to create a compact multiple layer flat plate OHP.

A 7-turn tubular oscillating heat pipe (T-OHP) was created and tested experimentally with three working fluids (water, acetone, and n-pentane) and different orientations (horizontal, vertical top heating, and vertical bottom heating). For vertical, T-OHP was tested with the condenser at 0°, 45° and 90° bend angle from the y-axis (achieved by bending the OHP in the adiabatic) in both bottom and top heating modes. The results show that T-OHP thermal performance depends on the bend angle, working

fluid, and orientation. Another design of L-shape closed loop square microchannel (750 x 750 microns) copper heat pipe was fabricated from copper to create a thermal connector with thermal resistance < 0.09 ˚C/W for electronic boards. The TC-OHP was able to manage heat rates up to 250 W. A laser powder bed fusion (L-PBF) additive manufacturing (AM) method was employed for fabricating a multi-layered, Ti-6Al-4V oscillating heat pipe (ML-OHP). The 50.8 x 38.1 x 15.75 mm^3 ML-OHP consisted of four inter-connected layers of circular mini-channels, as well an integrated, hermetic-grade fill port. A series of experiments were conducted to characterize the ML-OHP thermal performance by varying power input (up to 50 W), working fluid (water, acetone, Novec^{TM} 7200, and n-pentane), and operating orientation (vertical bottom-heating, horizontal, and vertical top-heating). The ML-OHP was found to operate effectively for all working fluids and orientations investigated, demonstrating that the OHP can function in a multi-layered form, and further indicating that one can ‘stack’ multiple, interconnected OHPs within flat media for increased thermal management.

DEDICATION

This dissertation is dedicated to my parents, family, and my best friend Rita Burrell for their support in every step of the way.

ACKNOWLEDGEMENTS

I would like to express my sincere appreciations to my advisor Dr. HeeJin Cho and my committee members: Dr. Pedro Mago, Dr. Yucheng Liu and Dr. Shanti Bhushan for their support and guidance. I would like to acknowledge Dr. Scott M. Thompson and my friend Dr. J.G. Monroe for their support and advise. I also would like to thank Dr. Lori Bruce, Dr. Masoud Rais-Rohani, Dr. Kari Babski-Reeves, Dr. Kalyan K. Srinivasan, Dr. Mark F. Horstemeyer, Dr. Haitham El-Kadiri, Dr. Douglas Bammann, Dr. Hossein Toghiani, and other faculty and staff members in ME for their instruction, help, patience, and kindness throughout my graduate study.

The research below would not have been successful without the financial support of the Bagley College of Engineering at Mississippi State University.

My sincere thanks to Zack Aspin, Shahzaib Abbassi, Colin Mahoney, Govinda Mahajin and all other present and past friends for unending support.

TABLE OF CONTENTS

LIST OF TABLES

LIST OF FIGURES

CHAPTER I

INTRODUCTION

1.1 The Oscillating Heat Pipe

The miniaturization and enhancement of electronics packaging schemes continue to challenge the design and engineering of compact heat dissipation systems for thermal management [1]. With heat fluxes nearing 1 kW/cm² being realized, conventional, single-phase thermal management techniques are no longer viable. This has resulted in disruptive technology innovations such as near-junction/intra-cooling [2,3] and two-phase, (far-junction) surface-mounted heat spreaders/sinks [4,5]. With regard to 'far-junction' thermal management, methods are continually sought for effectively spreading thermal energy from relatively thin media to maintain near-isothermal surfaces opposite to adjoined heat sinks. One such device for high heat flux thermal spreading is the thermal ground plane (TGP). The TGP is a surface-mounted, two-phase heat spreader that operates passively [3,6,7], relying on capillary structures such as porous/sintered media and mini/micro-channels for cyclic fluid pumping. Some examples of TGPs include flat heat pipes, vapor chambers, oscillating (or pulsating) heat pipes (OHPs) and other hybrid two-phase cooling technologies [5,8–12]. The mounting of a TGP typically requires that minimal stress occur at the source-contacting interface to ensure minimal damage to heat-dissipating electronics. To this end, the heat source and TGP coefficient

of thermal expansion (CTE) are often sought to be 'matched' for reducing interfacial stresses.

OHP's were invented by Akachi in 1990 [13] and have been used as a simple, compact, and efficient cooling device for electronics and other industrial applications. The OHP, as shown schematically in Figure 1.1, is a partially-filled capillary structure that meanders, in a serpentine-fashion, through a heat source (i.e. evaporator) and heat sink (i.e. condenser) [14,15]. It can take the form of media-embedded, mini/micro-scale channels (i.e. a flat plate OHP a.k.a. FP-OHP) or capillary tubing (i.e. a tubular OHP); each requiring a hermetic seal for optimal operation. Upon introduction of a sufficient temperature difference or heat flux, the fluid inside the OHP vaporizes and expands unevenly along various sections of its evaporator resulting in its 'start-up'. Vapor pressure builds due to sensible heating and results in a non-uniform, oscillatory pressure field forming against liquid volumes. The oscillatory fluid motion, combined with phase-change heat transfer, allows for cyclic, fluid-driven heat transport from the OHP evaporator to the condenser. This cyclic phase change is typically evidenced by an OHP surface temperature field that oscillates with respect to time [16,17]. The type and amount of working fluid, channel/tube dimensions, number of channel/tube turns, operating orientation with respect to gravity, and heating/cooling areas are some of the many design/operating parameters affecting OHP thermal performance [18,19].

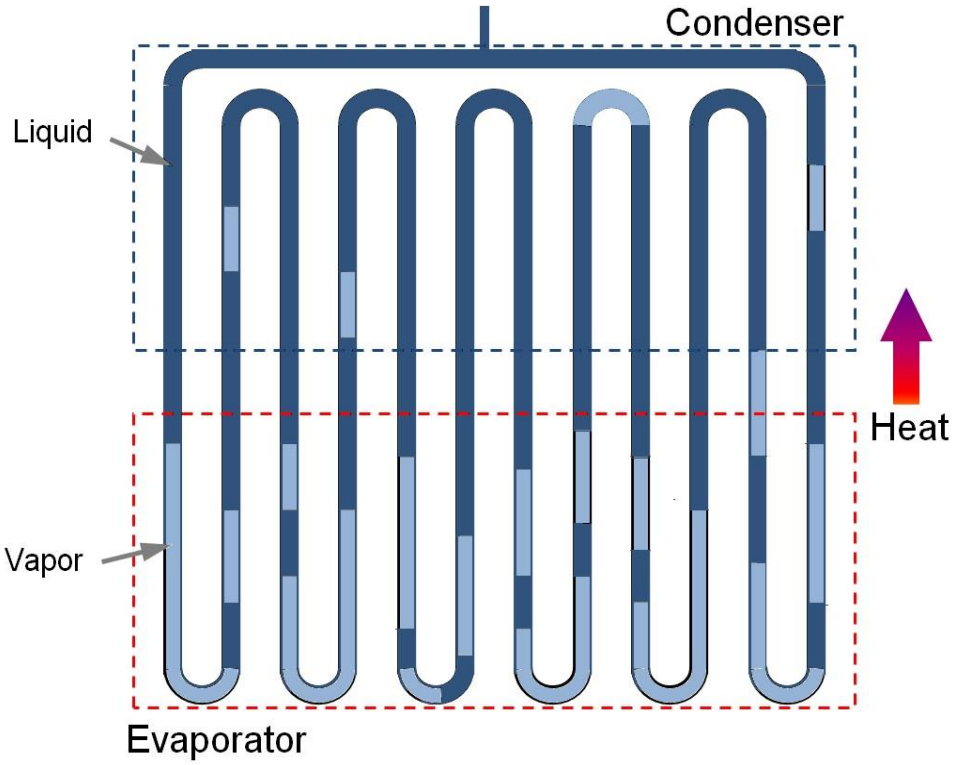

Figure 1.1 Schematic of typical liquid/vapor distribution within an oscillating heat pipe (OHP) consisting of uniformly-sized evaporator and condenser.

OHP is different from conventional heat pipes in that OHP oscillating flow is thermally driven combined with capillary forces [14]. Also, OHP has low pressure drop because the internal surface of the channels has no wicking structure. In contrast, the process of cooling in conventional heat pipe starts from boiling the working fluid in the evaporator, which causes vapor to flow to the condenser; the condensate then flows back to evaporator section through the wicking structure. However, the vapor bubbles generated inside the OHP evaporator section work as a driving force for the working fluid to reach condenser. When vapor bubbles reach condenser, they will condense and return back to the evaporator due to differences in pressure with adjacent channels (which can be aided by the effect of gravity if properly oriented). The OHP internal diameter is thus

crucial for this capillary behavior. The empirically derived critical diameter for sustained OHP operation is shown in equation (1.1).

$$d_c \leq 2 \left[\frac{\sigma}{(\rho_l - \rho_v) * g}\right]^{\frac{1}{2}} \quad (1.1)$$

The cyclic phase change of the working fluid inside the encapsulated serpentine tubes/channels causes sensible heat transfer, which actually represents the vast majority of the total heat transfer in an OHP [14].

The heat flux supplied on the evaporator and the heat dissipation from the condenser are the boundary conditions driving OHP operation [20]. Working fluid motion will not be sustained inside the OHP until a critical 'start-up' heat input is surpassed (although an initial fluid rearrangement may occur even at very low heat inputs). The start-up and oscillation of the working fluid between the OHP heat source section (evaporator) and heat sink section (condenser) depends on three forces: surface tension, gravity, and oscillation force which come from the pressure fluctuation between evaporator and condenser [21]. The parameters, which can affect working fluid motion and ultimately OHP performance, can be grouped into three categories: geometrical parameters, operational parameters, and physical parameters.

Furthermore, OHP designs can be grouped into three basic categories: 1) tubular oscillating heat pipe (T-OHP), which consists of capillary serpentine tubes as shown in Figure 1.1, 2) flat plate oscillating heat pipe (FP-OHP), which consists of micro-channels engraved on a metallic plate as shown in Figure 1.3, and 3) multiple layer oscillating heat pipe (ML-OHP), which is manufactured using selective laser melting additive manufacturing technology as shown in Figure 4.1 [22].

1.1.1 Tubular Oscillating Heat Pipe

A tubular oscillating heat pipe (T-OHP) is made from a serpentine capillary tube. T-OHP can be shaped into four different main designs: closed end, closed loop, closed loop with check valve and open loop as shown in Figure 1.2 [23]. Because of their simple geometry, T-OHPs are typically cheaper and easier to manufacture than FP-OHPs or ML-OHPs.

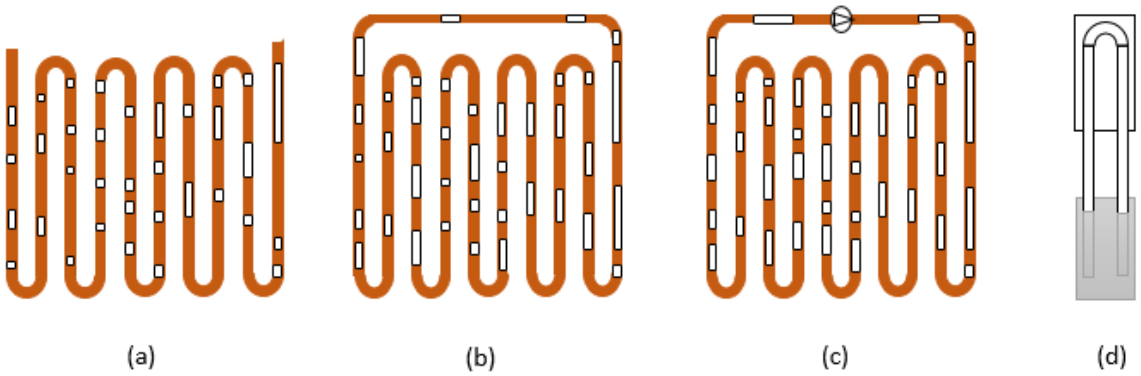

Figure 1.2 Different design of OHPs: (a) closed end (b) closed-loop (c) closed loop with check valve (d) OHP with open ends

1.1.2 Flat Plate Oscillating Heat Pipe

Flat plate oscillating heat pipes (FP-OHP) are manufactured by machining serpentine-arranged mini/micro-channels into a flat plate and then sealing the machined plate with a cover plate as shown in Figure 1.3. Copper, brass, aluminum, or other semi-conductive materials are typically used as a base plate for the FP-OHP, but any material capable of maintaining a hermetic seal can be used. FP-OHPs have larger surface contact ratios than T-OHPs due to the inter-channel material, which makes FP-OHP more desirable for high heat flux applications.

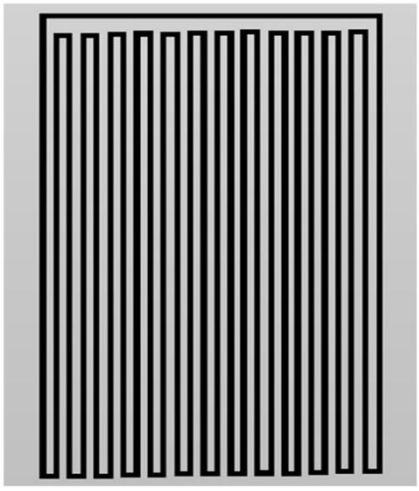

Figure 1.3 Flat plate microchannel oscillating heat pipe

1.1.3 Multi-Layered Oscillating Heat Pipe

The number of channel layers is of interest for high heat flux thermal management, since this allows the OHP channels to overlap themselves, which creates denser channel structures. Traditional OHP designs consist of a channel structure that remains in one plane, while multi-layered OHPs (ML-OHPs) consist of a channel that meanders through multiple planes. By having a multi-directional channel structure, the ML-OHP can be less prone to gravity or orientation dependence and thus provide for a wider range of heating/cooling boundary conditions [24].

1.2 Parameters Affecting Performance of Oscillating Heat Pipe

Oscillating heat pipe thermal performance is affected by many parameters, such as number of turns, evaporator and condenser design, channel geometry, orientations, charging ratio, working fluid, and others. In this study, different parameters were studied to find the operating limitations of different OHP designs.

1.2.1 Geometrical Parameters

OHP channels/tubes inner diameter is one of the geometrical parameters which affects the performance of OHP. In order for liquid slugs and vapor plugs to develop inside T-OHP channels, the inner diameter has to be sufficiently small, e.g. 0.5-3 mm. However, OHP theoretical analysis shows that the larger inner diameters could work under microgravity [25]. Charoensawan et al. [24] concluded that increasing the inner diameter of OHP at a specified temperature gradient between evaporator and condenser will increase its performance.

Sakulchangsatjatai et al. [26] determined that increasing the inner diameter of closed loop and closed ends OHP charged with R123 and heated from the top will increase the heat flux predicted from the model. For horizontal orientation, many investigations have been conducted to determine the parameters which can affect OHP performance. Rittidech et al. [27] experimentally tested closed end loop OHP charged with R123 at horizontal orientation and the results show that increasing the inner diameter will increase the heat flux. However, using ethanol as a working fluid in the heat pipe gave opposite results. Horizontal closed loop OHP thermal resistance decreases as the inner diameter increases by using water as a working fluid [28], but thermal resistance increases as the inner diameter increases by using ethanol as a working fluid. Rittidech et al. [29] used closed loop OHP with check valves and concluded that heat flux increases no matter whether water, ethanol or R123 was used as a working fluid. Cross-sectional shape of OHP is another geometrical parameter which affects the performance of OHP due to the effect of sharp angled corners [30]. Also, the cross-sectional shape of OHP has an effect on the start-up characteristics of OHP [20]. The

thermal resistance of OHP with variable diameters is higher than others with uniform diameter[31].

1.2.2 Effect of Orientation

Gravity has a significant effect on OHP heat transfer performance [32], although the impact factor of the working fluid inside oscillating heat pipe channels stronger than gravity. OHP thermal performance with bottom-heating (i.e. vertical) orientation is typically better than horizontal, where gravity helps the working fluid to oscillate by returning liquid to the evaporator [33]. Ma and Zhang [34] studied the effect of charging ratio and inclination angle on OHP thermal performance. Their results show that inclination angle has a significant effect among other variables. However, Yang et al.[30,35] concluded that the effect of orientation is insignificant with a decreased tube inner diameter where capillary forces are dominate.

1.2.3 Effect of working fluid

OHP capillary structure has to be filled partially with a working fluid in the range between 20-80% [19]. The working fluid is the foundation of OHP, where it works to transport heat from evaporator to condenser section. Working fluid selection depends on its surface tension, liquid and vapor densities, and the range of operating temperatures, where OHP critical inner diameter is a function of those parameters as shown in Equation 2.1. Some working fluids have high surface tension, which works to increase OHP critical diameter and pressure drop in the tube. Fluids with low latent heat work to evaporate liquids quickly at certain temperature, increase vapor pressure, and finally improve OHP thermal performance. Specific heat of liquids also important for OHP

performance, where it acts to increase sensible heat transferred [19]. Shear stresses reduce for working fluids with low viscosity [19]. Density and surface tension of a working fluid affect channel size of OHP for micro gravity [36,25]. Taft et al. [37] verified that surface tension, density and latent heat of vaporization of working fluid have a direct effect on the OHP start-up. By studying the effect of using acetone, n-pentane and Novec 7200 working fluids on the performance of multi-layer Ti-6Al-4V additive manufactured OHP, it will be shown in this work that working fluid has an important effect on OHP start-up and thermal efficiency.

1.2.4 Number of Turns

The number of turns has a direct effect on the heat transfer characteristics occurring in OHP between evaporator and condenser, with many studies being conducted to determine the optimum number of turns for various OHP designs. Sakulchangsatjatai et al. [26] concluded that the optimum number of turns for closed loop and closed end loop OHP must be more than 40 turns. The number of turns also has a relation with the operating time of OHP, where the average operating time of OHP increase as number of turn increase [38]. Charoensawan et al. [24] concluded that the critical number of turns depends on working fluid properties and tube inner diameter. In another research, Charoensawan and Terdtoon [28] found that the critical number of turns depends on evaporator temperature. Also, they concluded that the optimum performance of horizontal closed loop OHP occurs at 26 turns, which was the maximum number of turns used in the experiment.

1.3 The Objectives of This Study

The dissertation has three primary objectives: 1) a better understanding of the factors affecting the heat transport capability of the OHP in order to increase the efficiency; 2) develop an efficient OHP capable of working as a thermal connector for printed circuit boards; and 3) create simple, compact and efficient flat plate multiple layer oscillating heat pipe using selective laser melting. The following chapters encapsulate the research efforts focused on these objectives in a discrete manner.

Chapter II focuses on the thermal performance of a 7-turn tubular OHP, which was tested experimentally at horizontal and vertical orientations. OHPs can play an important role in heat dissipation for electronics, and in these applications, there is seldom a linear path between the heat source and sink. Thus, it is important to explore OHP behavior when the evaporator and condenser are not in the same plane. The tubular oscillating heat pipe (T-OHP) was tested for vertical orientation with the condenser at a 0°, 45° and 90° angle from the y-axis (achieved by bending the OHP in its adiabatic regions) in both bottom and top heating modes. At each angle, the OHP was tested with three working fluids water, acetone, and n-pentane. Power input was changed to record the starting point of oscillating, steady state, and the power where the maximum OHP temperature reached 100 °C. It was found that OHP works with vertical bottom heating and horizontal orientations for all bend angles but does not give the same performance with top heating. OHP performance at 90° angle bottom heating was better than other bend angles in all orientations. Furthermore, OHP performance was better with water working fluid than acetone and n-pentane for 45° and 90° angles, while acetone performed better at 0° angle.

Chapter III presents an L-shaped, closed-loop, square microchannel (750 x 750 microns) pulsating heat pipe that was fabricated from copper to make a thermal connector for electronic boards. The thermal connector was able to manage heat rates up to 250 W. Also, it included design features such as: i) easy removal and ii) a locking mechanism to secure the faces of the connector against the slotted water block. The experimental tests showed that the heat pipe thermal connector outperformed the solid copper control by maintaining a surface temperature 16 ℃ lower than the control at 250 W power input. The thermal resistance of the thermal connector decreased as heating power input increased to a minimum of 0.09 W/℃ at 100 W.

Chapter IV demonstrates using Selective Laser Melting (SLM), a type of additive manufacturing (AM) process, to fabricate a multi-layered oscillating heat pipe (ML-OHP) from titanium alloy (Ti-6Al-4V). The 50.8 x 38.1 x 15.75 mm^3, closed-loop OHP consisted of four inter-connected layers of circular mini-channels (1.52 mm). In order to discern the effect of the multiple layers on the thermal performance of the OHP, a series of experiments were conducted while varying the working fluid (water, acetone, Novec, and n-pentane – all at 70% fill ratios) and operating orientation (vertical bottom-heating, horizontal and vertical top-heating). The ML-OHP evaporator size was found to depend on the layer-wise heat penetration, which subsequently depends on power input and the ML-OHP design and material selection. Using neutron radiography, electron scanning microscopy, and surface metrology, the ML-OHP channel structure was characterized and found to possess sintered Ti-6Al-4V powder along its periphery. The sintered channel surface, although a byproduct of the L-PBF manufacturing process, would have behaved as a secondary wicking structure for enhanced capillary pumping and wall/fluid

heat transfer within the OHP. With the newfound capabilities of AM, many high heat flux thermal management devices, specifically those that employ mini- or micro-channels, can be ‘re-invented’ to possess embedded channels with a typical geometries, arrangements and surface conditions.

CHAPTER II

OSCILLATING HEAT PIPE PERFORMANCE AT DIFFERENT BEND ANGLES, ORIENTATIONS AND WORKING FLUIDS

2.1 Introduction

Utilizing a simple, compact and, efficient heat dissipation system is the target of all electronic designs. In this chapter, a 7-turn tubular OHP was shaped and tested experimentally to find the OHP thermal performance with various bend angles, orientations, and working fluids. The OHP was tested for horizontal and vertical orientations. For vertical orientation, OHP was tested at 0°, 45° and 90° condenser bend angle from y-axis as shown in Figure 2.1 (b). Water, acetone, and n-pentane were used at each bend angle. Horizontal orientation was tested with acetone working fluid at 0°, 45°, 90° and 135° bend angle. A T-OHP design was used as it is easy to manufacture and generate the bend angles between tests while maintained hermiticity. Furthermore, there is much existing research that investigates other T-OHP parameters.

Rittidech and Wannapakne [39] found that solar collector efficiency reached 62% by using 3 mm ID closed end loop copper circular tube oscillating heat pipe charged with R134a at 50%. Meena et al. [40] concluded that using closed loop OHP with check valves charged with R134a at 50% in air preheater increase heat transfer rate and effectiveness. Rittidech et al. [29] experimentally tested a 40 turn circular copper tube closed loop oscillating heat pipe charged with three working fluid (water, ethanol, and

R134a) at 90° inclination angle to the horizontal. It was found that the heat flux increased with an increase of the ratio of check valves and decreased with the increase of aspect ratio. Charoensawan and Terdtoon [28] studied experimentally the effect of increasing number of turns (5, 11, 16, and 26), using two working fluids (distilled water and absolute acetone) with three filling ratios (30, 50, and 80%) on the performance of a horizontal closed loop copper tube OHP. They concluded that the best performance occurred at the maximum number of turns. Wannapakhe et al. [41] found that the heat transfer rate of a 40-turn copper closed loop OHP with a check valve at different inclination angle (0, 20, 40, 60, 80 and 90°) was better by using silver nanofluid in comparison with pure water. Also, the best concentration of silver nanofluid was 0.5%. Lin et al. [42] studied the effect of silver nanofluid on thermal performance of closed loop OHP at variable filling ratios (20, 40, 60 and 80%) and different heating power (5 to 85 W in 10 W increments). They concluded that midterm values of 40% and 60% of filling ratio were better and the best is 60%. Maydanik et al. [43] did an experimental study to determine the efficiency of a 17- turn copper closed loop oscillating heat pipe (CL-OHP) with three variable heating orientations (90, 0, and -90°) and three working fluids (water, methanol, and R141b). They concluded that the top heating would not start up the CL-OHP. Chen et al. [44] developed a mathematical model to predict the thermal performance of a closed loop OHP charged with deionized water at 90° orientation. The effect of three sections on vapor condensation was precisely distinguished by the model. Line et al. [45] fabricated a polydimethylsiloxane OHP, which was tested with two different working fluids (methanol and ethanol) in vertical and horizontal orientations. The results showed that OHP in the vertical orientation worked better with methanol but

did not work properly with horizontal orientation. Qu and Ma [20] designed a glass OHP with circular channels charged with variable working fluids (water, methanol, ethanol, and acetone) at 90° orientation to predict the factors that can affect heat pipe performance. They found that start-up performance could be improved by using rougher surface, controlling vapor bubble type, and selecting right working fluid. Lin et al. [46] studied the effect of using three different working fluids (FS-39E microcapsule fluid, pure water, and ethanol) with different percentages of filling ratio (40-80%) and variable power input (0-80 W) on copper circular channel OHP start-up and thermal performance. The results showed that the start-up of OHP was dependent on the liquid filling ratio, thermal driving force, and working fluid. Yang et al. [35] studied the thermal performance and thermal resistance of two different inner diameters (1 and 2 mm) closed loop OHP at three orientations (90, 0, and -90°) charged with R134a. The OHP worked successfully with both inner diameters but thermal resistance for d_i = 2 mm was lower than d_i = 1 mm by 10%.

2.2 Oscillating Heat Pipe Prototype Design and Experimental Setup

A 7-turn oscillating heat pipe was fabricated from copper tubing (C12200 alloy) with d_i = 3.25 mm and d_o = 4.8 mm, as shown in Figure 2.1. The heat pipe was divided into three sections: evaporator, condenser and adiabatic. The heat pipe was evacuated to less than 100 Pa before it was charged with working fluid (water, n-pentane, or acetone) at 70 % filling ratio (+/- 2%). The charging tube was pneumatically crimped directly after charging to create a hermetic seal.

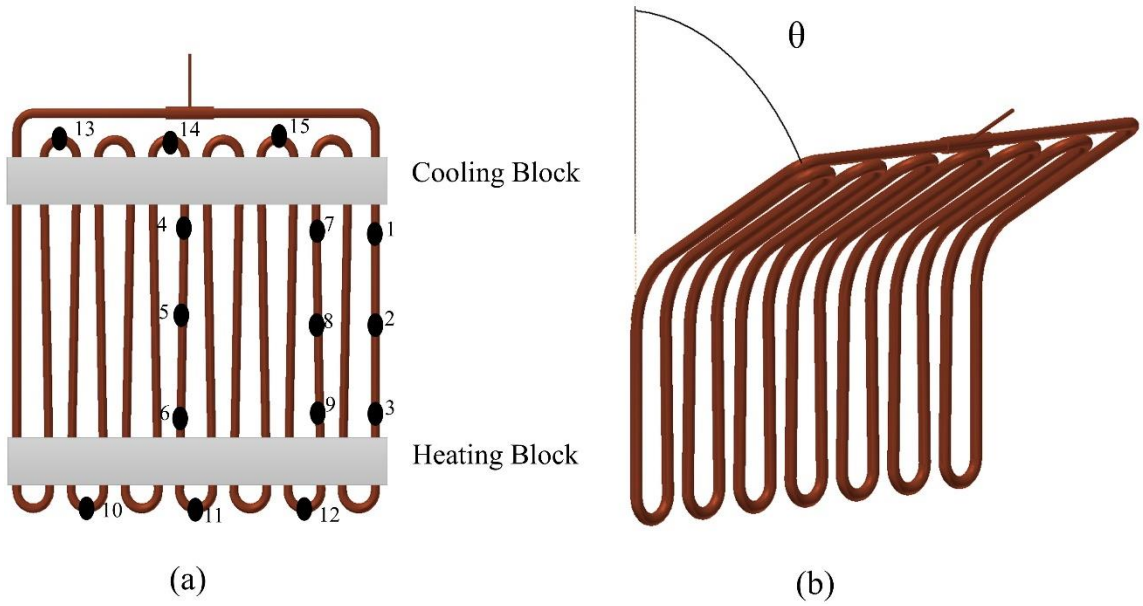

Figure 2.1 Tubular OHP (a) with thermocouple arrangement, heating and cooling blocks (b) bend angle

Pairs of cooling and heating aluminum blocks were made with grooves machined into their mating surfaces that matched the OHP tubes (2.4 mm radius). Before the blocks were fastened to OHP copper tubing, these grooves were coated with a thin layer of thermal paste (Omegatherm 201) to reduce the thermal contact resistance between aluminum blocks and copper tubing. The placement of the heating and cooling blocks created three OHP sections: evaporator, adiabatic, and condenser. The evaporator (*i.e.* heating block) and condenser (*i.e.* cooling block) sections had a length of 25 and 32 mm, respectively, while the distance between evaporator and condenser was fixed to be 75 mm. The total length of the OHP was 177 mm. The two aluminum cooling blocks were connected to a water circulator (PolyScience AD15R-30-A11B) to provide a 20 ºC cooling water, and two cartridge heaters 190 mm in length were placed inside aluminum heating blocks to heat the OHP using a variable autotransformer (Staco Energy), *i.e.*

variac, to control the power input. The variac connected with a digital multimeter (DMM) to measure the voltage output of the variac. Power calculations were based on cartridge heater resistance using $P=V^2/R$. The whole OHP test assembly was then wrapped in a fiberglass insulation to reduce heat losses to the atmosphere. In this experiment, heat losses were neglected in all calculations and it is assumed that all power supplied by the heater absorbed by the heat pipe and transited to the water blocks. However, some heat loss from the OHP existed and increased as the power increased. Based on the insulation surface temperature the percentage value of heat losses from the OHP at high power were estimated to be ≤5%. A schematic of the experimental setup is shown in Figure 2.2.

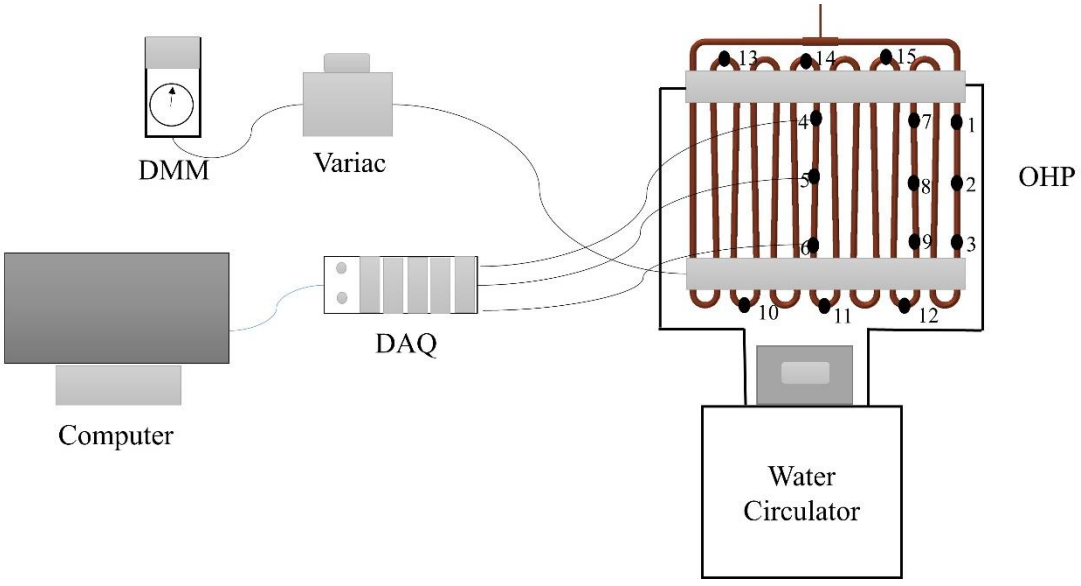

Figure 2.2 Tubular OHP in top heating mode connected with heating, cooling blocks, water bath, DMM, and variac.

Fifteen T-type thermocouples were attached to the outside wall of OHP tubes to obtain temperature data, which was collected using National Instruments cDAQ-9178 data acquisition (DAQ) system using NI-9213 temperature model. LabVIEW Signal

Express 2016 was used as the interface program to read and record the data collected by the DAQ. Power input was changed to record the starting point of oscillating, steady state, and the power at which the OHP reached 100 °C. The same experimental test procedure was repeated for both top and bottom heating orientation at OHP bend angles from 0° to 135° with 45° increments (see Figure 2.1b), where OHP bended by fixing the heat pipe with a bench vise then bend it carefully using shaft.

2.3 Results and Discussion

The bent tube oscillating heat pipe (BT-OHP) thermal performance can be quantified by calculating its thermal resistance. Thermal resistance was calculated by taking the average temperature difference between the evaporator (using T_3, T_6, and T_9 in Figure 2.2) and condenser (T_1, T_4, and T_7) and dividing by the power input to the heater, P, as shown in Equation 2.2.

$$\psi_{\mathrm{eff}} = \frac{(\mathrm{T_{evap}} - \mathrm{T_{cond}})}{\mathrm{P}} \tag{2.2}$$

Figure 2.3 shows BT-OHP performance with three different working fluids (water, acetone, and n-pentane) and three different bend angles (0°, 45°, and 90°). BT-OHP thermal performance increases as bend angle increase, where the surface temperature of the OHP charged with water reaches 100 ℃ at ∼300 W power input at a 0° bend angle, 600 W at 45° bend angle, and 750 W at 90° bend angle. This observation is attributed to the condenser performing better as the bend angle increases since the gravity effect for the condenser section decreases as the orientation changes from vertical to horizontal. Also, the bend angle between the evaporator and condenser introduces a pressure drop that affects the oscillating flow coming from the evaporator and increases

the period of time for the working fluid to remain within the condenser. The bend angle works to decrease the perturbation in the condenser.

The BT-OHP performs better with acetone at 0° and water at 45° and 90° bend angles. Working fluid properties such as surface tension, latent heat of fusion, specific heat and viscosity have a direct effect on the performance of an OHP [19]. Low latent heat and viscosity of acetone make the oscillating velocity of liquid slug faster than water which has high latent heat and viscosity [19]. Working fluids with large specific heat like water start to be more effective than other working fluid parameters as bend angle increase, where bend angle work to damp the fluid oscillation velocity.

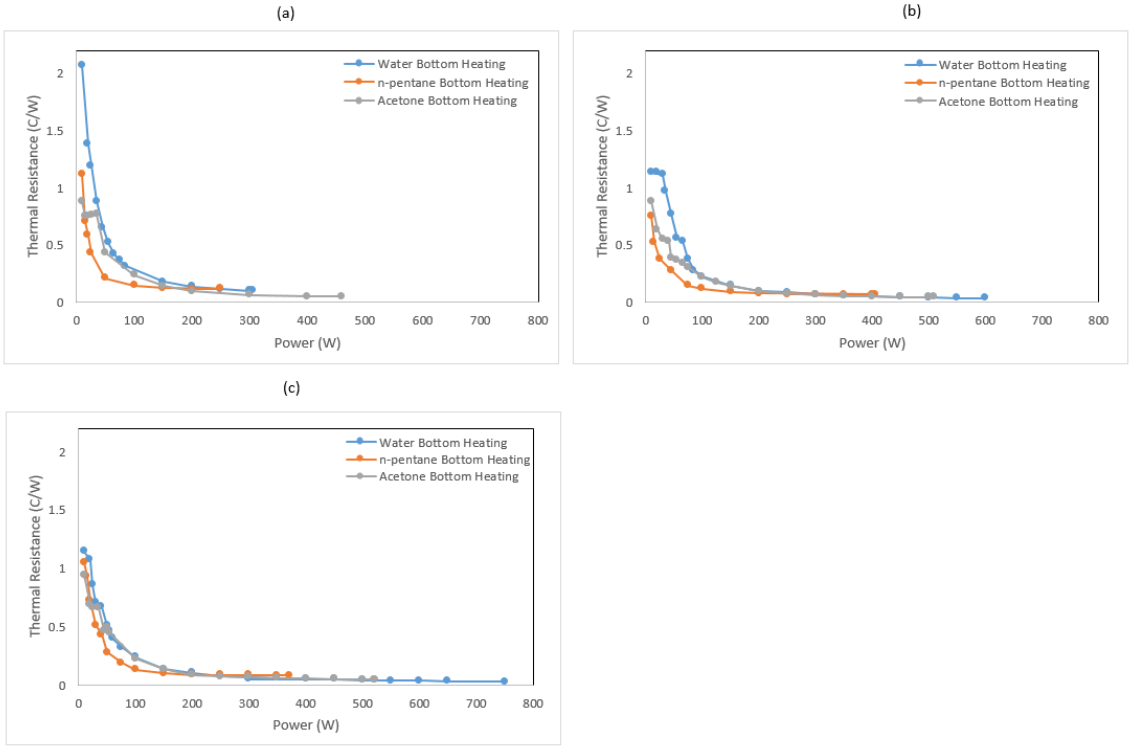

Figure 2.3 Power vs. Thermal resistance comparison between three working fluids (water, acetone, and n-pentane) with bottom heating orientation) at specific bend angle: (a) 0° (b) 45° (c) 90°.

Figure 2.4 shows the thermal performance of BT-OHP charged with acetone at different bend angles (0°, 45°, 90°, and 135°) and different orientations (vertical bottom heating, vertical top heating and horizontal). BT-OHP thermal resistance was plotted with variable power input at 0°, 45°, 90°, and 135° bend angles. From 0° to 90°, OHP performance with bottom heating orientation was better than top heating and horizontal. However, BT-OHP with 135° bend angle performed better in horizontal orientation than bottom and top orientations. Gravity improves the performance of any heat pipe operating while in the bottom heating configuration. For top heating, the performance of BT-OHP was lower than bottom and horizontal. That the working fluid dries out quickly more than other orientations. Whereas the surface temperature reached 100℃ at only 50 W power input while with bottom heating, it reached 525 W and 275 W for vertical bottom heating and horizontal orientations, respectively.

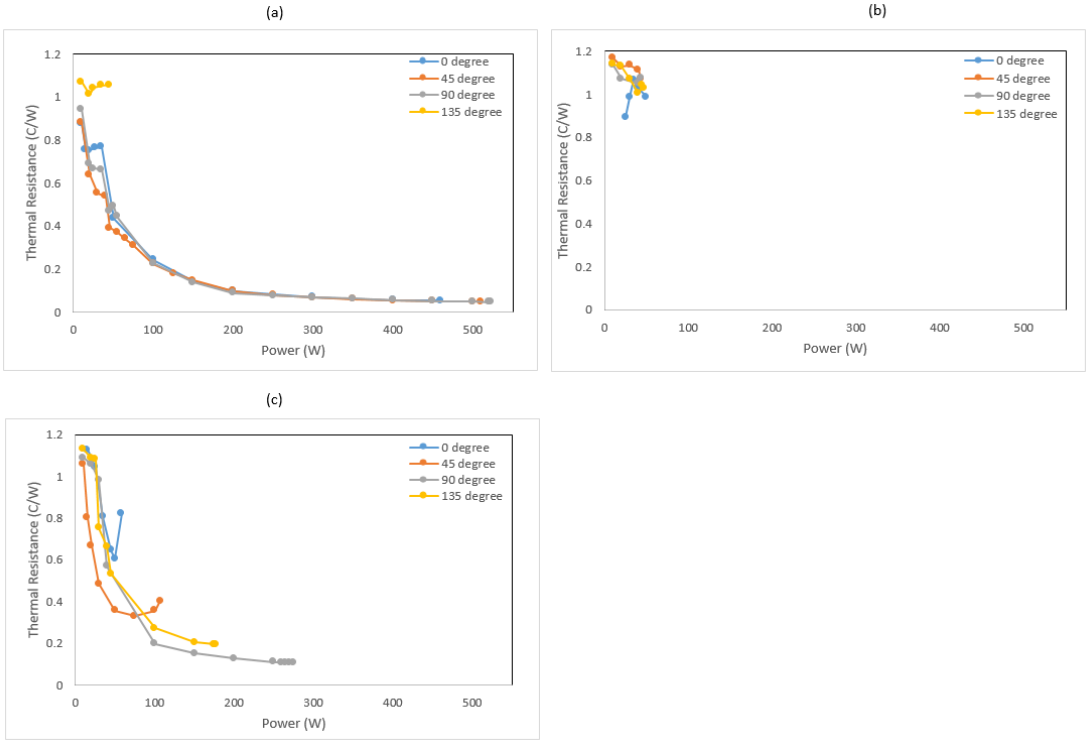

Figure 2.4 Power vs. Thermal resistance comparison between OHP bend angles for acetone working fluid at certain orientation: (a) Bottom heating (b) Top heating (c) Horizontal.

CHAPTER III

THERMAL CONNECTOR OSCILLATING HEAT PIPE

3.1 Introduction

Ever since the advent of integrated circuits, the challenges of electronic cooling have steadily increased. The high power densities of modern electronic designs result in high heat fluxes that can tax the capabilities of conventional forced convection cooling techniques. Electronic packages with complex designs can require novel thermal connectors to successfully transfer heat from the electronic components to system level cooling structures (*e.g.* forced air or liquid cooling) [1]. Mechanically, thermal connectors require some features to defend against vibration or thermal expansion compromising the contact between the connector and the heat source (which would increase the thermal resistance between the connector and source). Thus, the connector requires both a method of heat transport and a clamping mechanism for successful thermal mitigation.

3.1.1 Thermal Connectors

The earlier research on thermal connectors typically focused on the mechanical retaining mechanism[47 - 52]. Thermal issues may have been ignored in these earlier works due to the relatively low levels of generated heat of contemporary electronics. Wenz [53] investigated a coating material having properties of high thermal conductivity and low coefficient of friction between the heat sink strips on the edge of the board and

the frame member. Pesek [54] invented a wedge technique to protect the PCB from vibration and dissipate heat generated from the board to the chassis. Yousif and Kolbrekken [55] proposed a wedgelock and oil based ferrofluid interface material to reduce the thermal resistance between electronic board and cold block. The results show that using ferrofluid material is better than wedgelock. Rank and Whalen [56] invented a hydraulic thermal clamp includes a series of internal hollows along a screw to pass through carried by a jackscrew, this device works to fix the board and dissipate heat generated. Reilly et al. [57] designed a wedgelock of aluminum triangular pieces to provide a locking force and transfer heat from the board to the cooling plate. The Defense of Advanced Research Projects Agency (DARPA) and the office of Naval Research hosted a competition for the years between 2012 to 2015 promote the advancement of thermal connector technology. The competition design has aluminum heating plate provided with a heater and aluminum cooling block with longitudinal channel connected with water circulator. The purpose of the competition is to get a thermal connector having the capability of applying a clamping force on the hot plate with the cooling block and works to reduce the thermal resistance between them. Through a series of progressively more difficult challenges, the initial field of designs was down-selected to four prototypes that were then externally tested by industry experts. Georgia Tech developed a hydraulic thermal connector provided with a screw which works to apply a force on the honey working fluid inside the copper series and exert a pressure on the piston due to its volume change occurs in the honey [58]. The University of Missouri Columbia used direct laser centering to fabricate two wedges thermal connector. Also, they were created a stainless-steel pulsating heat pipe thermal connector using direct metal sintering [58]. National

Tsinghua University proposed a thermal connector with front and rear wedges [58]. The University of Maryland delivered two pieces wedge with an end screw, in which end screws push two wedges laterally for clamping purposes [58]. The University of California-Merced designed a three wedge device which works to provide the clamping force [58].

3.1.2 Features of Thermal Connector Oscillating Heat Pipe

The oscillating (or pulsating) heat pipe (OHP), as shown conceptually in Figure 1.1, utilizes temperature-actuated, oscillating flow for thermal management in a variety of applications. When a temperature difference is imposed across the length of the serpentine OHP channels, non-uniform vapor expansion in the evaporator (*i.e.* area of heat reception) increases until, after a sufficient driving temperature difference is achieved, the quasiperiodic motion of the internal vapor and condensate occurs. This oscillating pressure field provides the mechanism for the replenishment of vapor in the condenser (heat sink location) in order to sustain its cyclic operation without a wick structure. Relative to other heat pipes, the OHP can be miniaturized and costs less to manufacture. The OHP tube/channel structure has a capillary dimension (~ 1 mm) to form stable liquid plugs during operation.

The OHP working fluid is selected based on the power range of the described application; oscillations should start at bottom of the range and evaporator dry out (*i.e.* OHP operational limit) should not interfere at top of range. Qu and Ma [20] presented an equation for the start-up heat transfer of an OHP, $q_{\min}$, which incorporates vapor bubble growth due to nucleate boiling:

$$q_{\min} \approx \frac{k_l T_v A_{c,h}}{r_i \ln[r_i/(r_i-\delta_l)]} \left(1/\left\{1 - \frac{RT_v}{h_{lv}} \ln\left[1 + \frac{2\sigma}{p_v R T_v r_n}\right]\right\} - 1\right) A_{c,h} \quad (3.1)$$

Where r_i is the internal radius of the OHP mini-channel and $A_{c,h}$ is the cross-sectional area of the mini-channels in the evaporator. Based on Equation 3.1, a number of working fluid and material properties are of interest for minimizing the start-up heat input of the OHP. The liquid thermal conductivity, k_l, and latent heat of vaporization, h_{fg}, should be minimized, and the surface roughness of the internal channels (depth of nucleation sites), r_n, should be maximized. The start-up heat input equation dictates working fluid selection, filling ratio and material roughness. Equation (3.1) led to Novec 7200 (3M) being selected as the working fluid since it has a low latent heat of vaporization and high vapor pressure.

A 2-piece, Oscillating heat pipe thermal connector (TC-OHP) was manufactured by machining a closed-loop square microchannel (750 x 750 microns) into a copper substrate. The goal of the TC-OHP prototype was to design a thermal connector with thermal resistance < 0.09 ˚C/W for electronic boards. The milled channel is reminiscent of traditional FP-OHPs, however, the channel structure of the TC-OHP was L-shaped, not planar like other FP-OHPs. This design shift required the development of a new brazing technique. The thermal performance of the TC-OHP is shown to be superior to that of the solid copper control thermal connector. Furthermore, this work demonstrates the feasibility of a new OHP form factor applicable to small scale or geometrically complex thermal management issues.

3.2 Thermal Connector Prototype

3.2.1 Design and Manufacturing

The thermal connector, shown unsealed in Figure 3.1, is CNC machined from solid blocks of copper alloy 110. The connector consists of two opposing wedge-shaped sections: the primary section containing the intricate micro-tube pulsating heat pipe filled with a working fluid and sealed by brazed cover plates, and the secondary portion to function as the wedge. A steel shaft is threaded into the thickest portion of the main section of the TC-OHP and extends lengthwise along the TC-OHP. A slot and hole in the secondary portion (visible in Figure 3.1) allow the steel rod to act as a connecting rod to hold the two parts together. The wedging action is performed by tightening a nut on the unsecured end of the connecting rod, forcing the secondary portion of the TC-OHP inward.

Combined dimensions of the two copper sections include a nominal length of 150 mm, height of 12.7 mm, and a nominal width of 6.35 mm when fit together. The connecting rod is a 3.175 mm diameter, 4-40 threaded steel rod. The length and width of the assembly will change as the fastener on the connecting rod is tightened.

The pulsating heat pipe consists of 13 micro-channel loops on the evaporator side (visible in Figure 3.1) and 12 micro-channel loops with a “return” channel on the condenser side. The channels on the evaporator side have a hydraulic diameter of approximately 0.76 mm while the channels on the condenser side have a diameter of 1.01 mm. The changing diameter encourages fluid flow as fluid expands within the evaporator and is forced into the higher volume condenser.

Due to the angled design of the TC-OHP, a novel brazing method had to be devised. An angled brazing chassis was developed so both the evaporating and condensing sections of the TC-OHP could be brazed simultaneously. The bottom of the chassis holds the TC-OHP in place while a second part is placed on top of the TC-OHP allowing the additional weight to be applied to the assembly to ensure proper contact for brazing. These components can be seen in Figure 3.2.

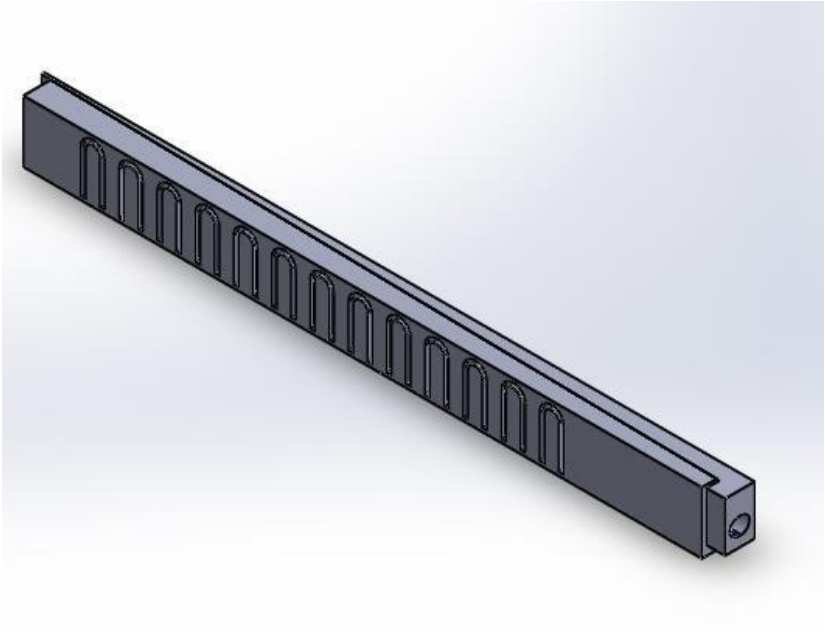

Figure 3.1 Two-piece thermal connector with embedded oscillating heat pipe (unsealed)

Figure 3.2 Brazing Chassis with Test Connector

To prepare the TC-OHP for brazing, the surfaces of the primary portion and the cover plates that were to be brazed were prepared by softly sanding. The connector, the cover plates, and the braze foil were then thoroughly cleaned by being submerged in a bath of cleaning solution to cleanse the surface of any impurities and oxidation. The brazing chassis, with the connector, braze foil, and cover plates in place was then placed within a controlled atmosphere brazing furnace. For this application, the brazing furnace was continuously purged with argon to ensure no oxidation of the connector occurred during the brazing process.

3.2.2 Prototype Strengths and Weaknesses

The simple 3 piece design makes the OHP an attractive choice as a thermal connector. It is easily installed and removed using basic hand tools. However, the delicate nature of the copper sheet that seals the OHP is a concern if the assembly were to be

deformed or otherwise damaged. If the sheet was to rupture, the hermetic seal would be lost resulting in the OHP ceasing to function. The performance of the thermal connector would then be solely dependent of the thermal conduction of copper. Furthermore, the TC-OHP requires complete contact with the bottom of the channel in which it is inserted for the OHP to fully reject heat from the condenser. Any air gap will form an insulating layer effectively increasing overall thermal resistance.

3.3 Experimental Setup and Procedure

The experimental setup consists of a machined aluminum block to function as a cold thermal sink (the cold block). This block features multiple channels through which temperature controlled water is circulated and 12.7 mm square channels for testing the TC-OHP (see Figure 3.3). Heat is supplied by a resistive heater mounted in the center of an aluminum plate which will loosely simulate a PCB. Power input to the resistive heater is controlled by a Variac and measured by a digital multi-meter (DMM).

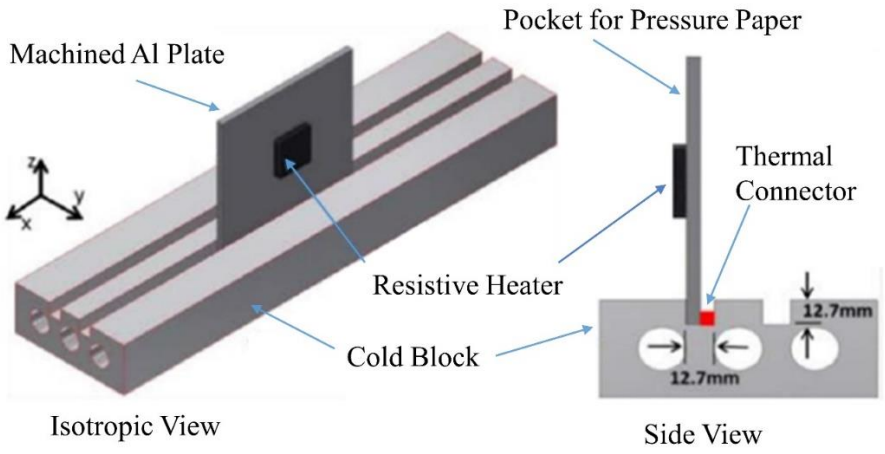

Figure 3.3 Thermal Connector Setup with The Cooling and Heating Blocks

The aluminum plate and the TC-OHP are fully inserted into one of the slots in the cold block such that the evaporator portion of the OHP is against the plate and the condensing portion is in full contact with the bottom of the slot. Multiple thermocouples are attached to the aluminum plate, the cold block, and the TC-OHP to accurately analyze the thermal performance of the system. The data is collected using a National Instruments Data Acquisition System (DAQ) and compiled in Microsoft Excel. Visual results displayed through Simulink Express provide real-time insight to the behavior of the system, as well as oscillation of the heat pipe mechanism of the thermal connector. The full experimental setup is illustrated in Figure 3.4.

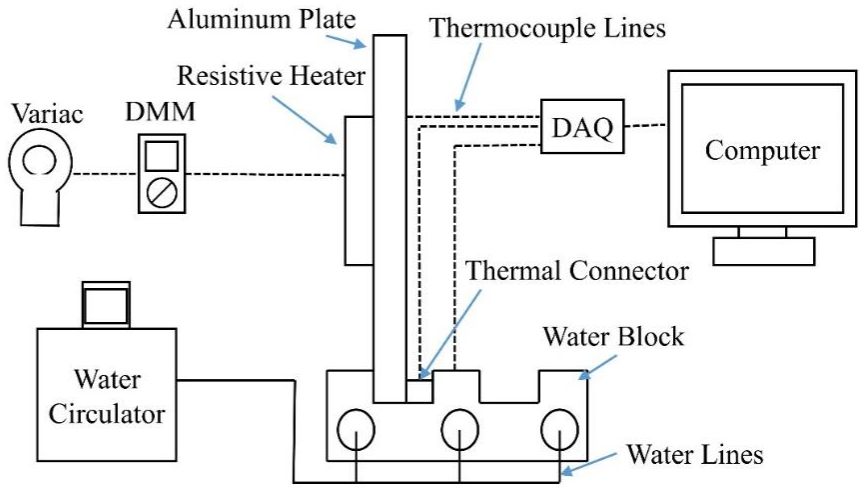

Figure 3.4 Experimental setup for characterizing the TC-OHP

Prior to insertion into the slot, the heat pipe was full evacuated using a vacuum pump and charged with Novec 7200 to a fill ratio of 70%. This was determined by calculating the internal volume of the TC-OHP and carefully weighing it during the charging process.

Throughout testing, 20°C cooling water was supplied continuously through the cold block. The tests were initiated when the entire insulated test assembly reached equilibrium with the circulated water. The experimental setup was then stepped through pre-determined inputs ranging from 0-250 watts by controlling the voltage to the heating plate using a Variac. The voltage needed to provide the specified power levels was found using Ohm's Power Law and the resistance of the heater which was measured to be 47 ohm. Steady state data was recorded at 25, 100, 150, 200, and 250 watts for 30 seconds at each interval.

OHP thermal performance was calculated by taking the average temperature difference between the evaporator and the condenser and dividing it by the power input. The test was repeated three times with proper contact between the condensing section of the TC-OHP and the bottom of the slot in the cold block and two times without ensuring proper contact to demonstrate the effects of improper insertion. These results are shown in Tables 3.1 and 3.2.

Table 3.1 OHP thermal resistance for a proper and improper insertion of the TC-OHP.

	Proper Insert			Improper Insert	
Power	OHP1	OHP2	OHP3	OHP4	OHP5
25	0.07078	0.083467	0.067768	0.124475	0.11685
100	0.08559	0.088696	0.082527	0.127624	0.120652
150	0.08479	0.087791	0.082721	0.120832	0.114679
200	0.08371	0.084765	0.081037	0.113836	0.109272
250	0.08272	0.086249	0.07954	0.110407	0.108329

Table 3.2 Control thermal resistance for a proper and improper insert between hot and cold blocks

	Proper Insert	Improper Insert	
Power	Control 1	Control 2	Control 3
25	0.107762	0.14079	0.143927
100	0.119448	0.14738	0.151072
150	0.117595	0.14597	0.151216
200	0.116127	0.14687	0.147336
250	0.114992	0.14707	0.145431

3.4 Results and Discussion

Following the process detailed above, the results show that 16°C temperature difference was measured between the connector and the control when operating at 250W. The steady state temperatures can be seen below in Figure 3.5.

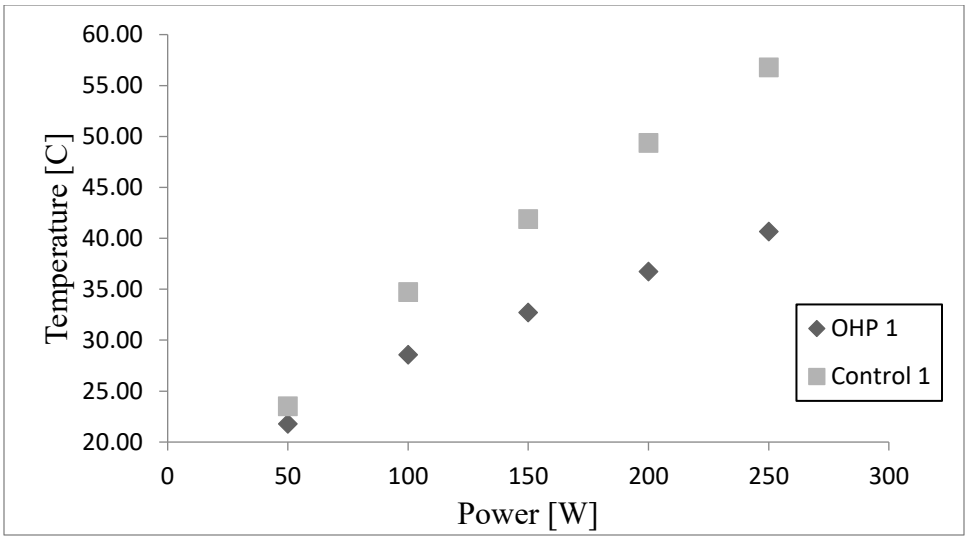

Figure 3.5 Steady state temperature distribution vs. power input comparison between heat pipe thermal connector and control.

It can be seen from Figure 3.5 that the connector performs increasingly better than the control with higher power inputs. To further analyze the initial data, the thermal resistance was calculated as follows for each power level:

$$\psi = \frac{T_{ss,avg} - T_{water}}{Power} \tag{3.3}$$

The result of this analysis is shown in Figure 3.6. These results demonstrate that the thermal resistance of the connector is an order of magnitude lower than the control. Furthermore, the thermal resistance of the connector decreases as temperature increases due to ever increasing activity in the OHP.

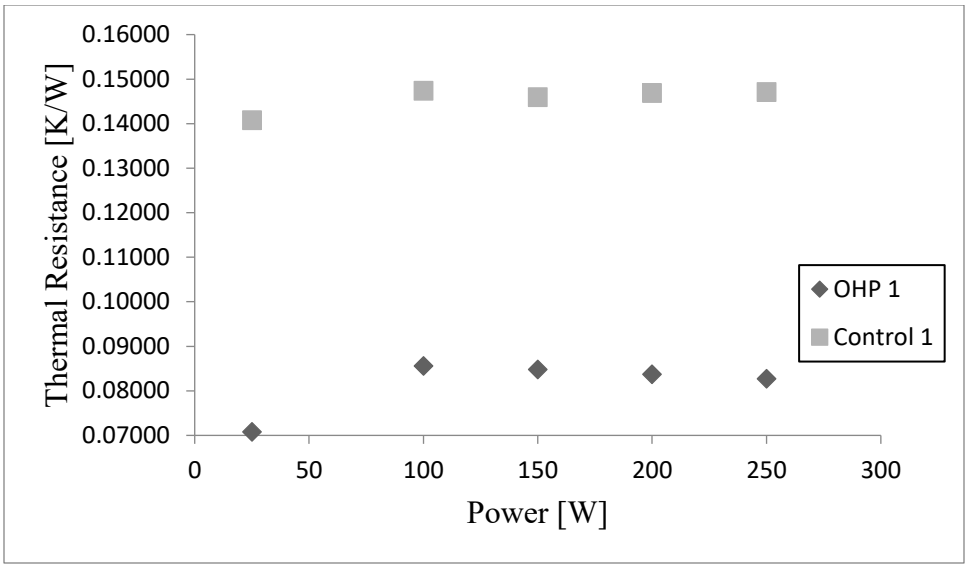

Figure 3.6 Thermal resistance vs. power input comparison between oscillating heat pipe thermal connector and control.

The connector uses the bottom of the channel as cooling for the evaporator region of the OHP. It was discovered that if the connector is not well inserted into the channel, sub-optimal thermal resistance will occur. It is theorized that a small air pocket under the evaporator region acts as an insulating layer against OHP's operation.

Two tests were run with the OHP improperly inserted into the channel. No special care was taken to ensure that it was well seated against the bottom. These tests resulted in higher thermal resistances than had previously been measured. The connecter was tapped down into the channel after the wedge was secured in place.

Similar tests were conducted on the control. Two tests were run with improper insertion, and one test was run while guaranteeing a proper fit to the bottom of the channel, as well as forcing the wedge in place until the material began to yield.

Several observations can be made from the results of these tests. In Figure 3.7, the comparison between the thermal resistance of the improper insertion of the connector and the improper insertion of the control can be seen.

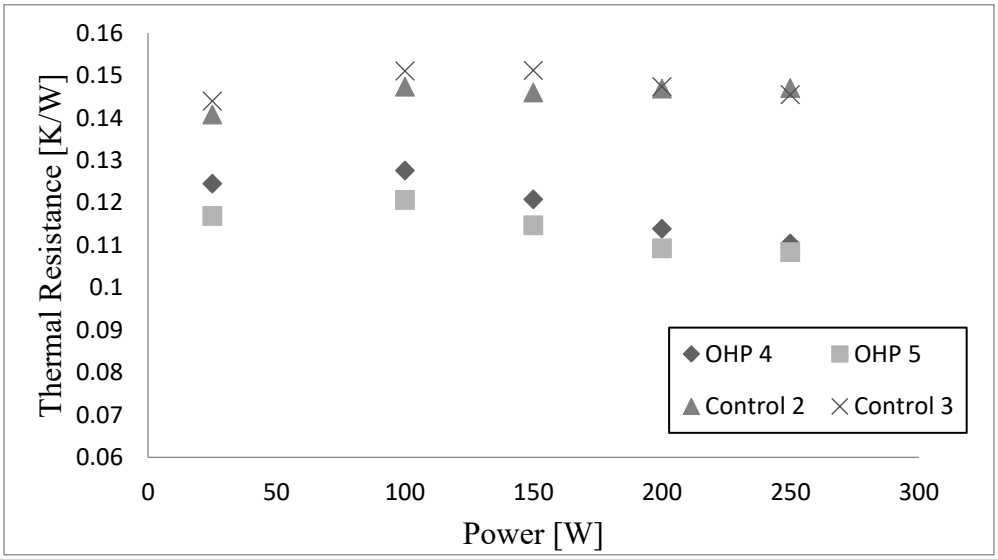

Figure 3.7 Worst Case Thermal Resistance.

This can be considered as the worst case scenario for both devices. The connector will not operate ideally as it does not have solid contact with the bottom of the channel, and the control cannot take full advantage of the bottom surface for conduction. Despite this being the worst case scenario, the connector performs from 11.6% to 26.3% better than a similarly inserted control.

In Figure 3.8, the best case scenario for both devices is displayed. The tests shown here ensure the devices are pressed against the bottom of the channel as well as held securely in place by the wedge.

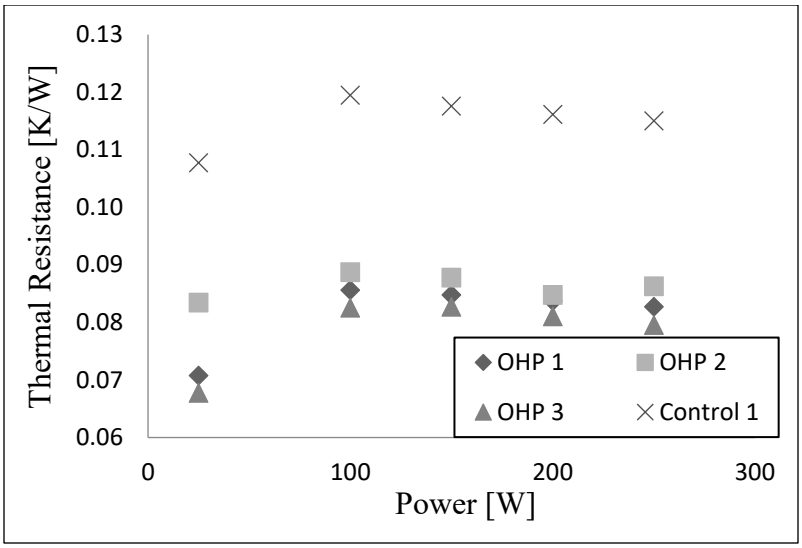

Figure 3.8 Best Case Thermal Resistance.

In this scenario, the connector is firmly seated against the bottom surface allowing proper operation of the condenser region. In this orientation, the connector has 22.5% to 37.1% lower thermal resistance than the control.

It is clear that in both scenarios that the OHP enhanced connector performs better than the control in similar conditions. It is worth noting that, at its worst, the connector performs as proper as the connector at its best as shown in Figure 3.9.

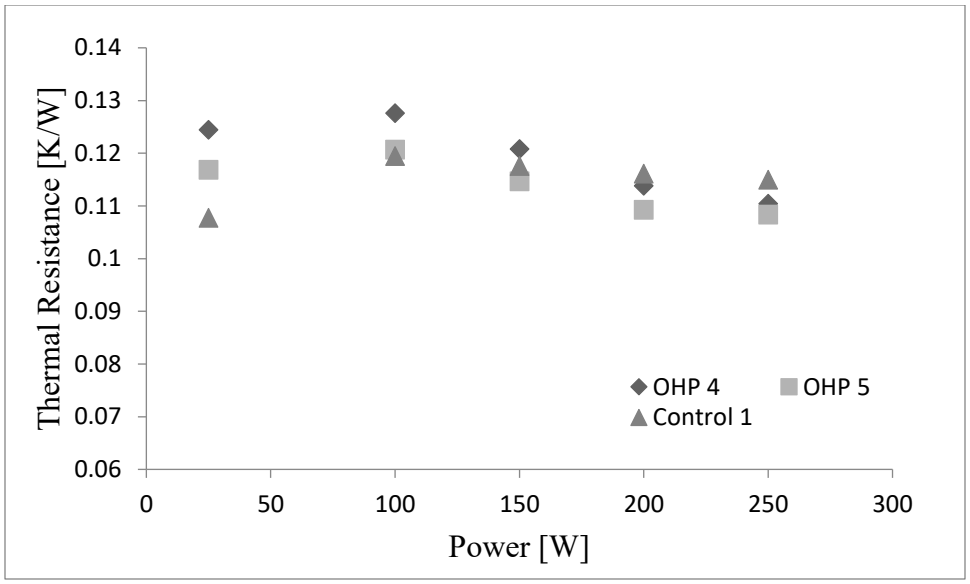

Figure 3.9 Worst Case Connector vs Best Case Control.

It can be inferred from this comparison that the connector will at worst behave as a solid piece of copper that is operating under ideal conditions

CHAPTER IV

MULTI-LAYERED OSCILLATING HEAT PIPE ADDITIVELY MANUFACTURED FROM Ti-6Al-4V POWDER

4.1 Introduction

The importance of passive and compact heat dissipation systems continues as electronic components continue to miniaturize and become more powerful. Flat heat pipes, or vapor chambers, and other sintered media and mini-channel technology, are some of the early passive devices used for cooling thermal systems [60-62]. For the high heat flux thermal management problem, surface-mounted but both have limit ability to dissipate high heat fluxes [63]. In 1990, the first oscillating heat pipe (OHP) was introduced. Unlike a vapor chamber, the OHP can dissipate high heat fluxes without dry out [18,19, 24,64-67]. Working fluid, filling ratio, OHP orientation, operating temperature, number of channel turns, heating/cooling area, and channel dimensions are the main parameters of the OHP thermal performance [18]. The oscillating heat pipe can be constructed from serpentine tubes or a flat plate with a closed-loop, meandering mini- or micro-sized channel (ML-OHP). The working fluid of the oscillating heat pipe is key to achieving high effective thermal conductivities by transporting the heat from evaporator to condenser through both sensible and latent heat.

The working fluid selected for the OHP must demonstrate wicking behavior as governed by the OHP channel/tube hydraulic radius, r_H, and operating environment (e.g.

gravity). Conditions for capillarity, and thus effective OHP operation, can be estimated via the Bond number, Bo, i.e.:

$$\mathrm{Bo} = \frac{r_{\mathrm{H}}^2 \Delta\rho_{\mathrm{lv}} g}{\sigma} \lesssim \mathrm{Bo_c} \tag{4.1}$$

where σ is the liquid-to-vapor surface tension, $\Delta\rho_{\mathrm{lv}}$ is the difference in density between the liquid and vapor phases, and $\mathrm{Bo_c}$ is the critical Bond number for capillarity and can range between 0.8 – 1.0 [15,36].

The thermophysical and rheological properties of the utilized working fluid dictate OHP thermal performance. A fluid's surface tension strongly influences evaporation heat transfer [68], as well as the pressure gradient along the OHP flow path [19]. Fluids with a lower latent heat of vaporization and dynamic viscosity tend to provide for slower flow speeds, moderate heat transfer, and lower OHP start-up powers [19,20,24]. A fluid's specific heat capacity influences its single-phase heat transfer during oscillatory, forced convection within an operating OHP. Since the majority of OHP heat transfer is typically sensible [69], the specific heat capacity and thermal conductivity are thus important thermal properties of the working fluid. A fluid with a vapor pressure highly sensitive to temperature is desirable for increasing an OHP's pumping capability – which is needed for assisting its start-up and consistent operation [19]. Taft et al. [70] demonstrated that the latent heat of vaporization, surface tension, and density of working fluids play an important role in OHP start-up and that viscous fluids provide more dampened temperature oscillations during OHP operation. Both the surface tension and density of a working fluid can affect OHP channel sizing for various micro-to-macro gravity environments (i.e. the Bo is gravity dependent) [25,36]. In general, fluids with low dynamic viscosity and latent heat of vaporization reduce the heat input required for

OHP start-up by minimizing channel pressure drop [19,70]. Fluids with a smaller latent heat of vaporization can improve OHP performance by providing higher oscillating velocities (caused via higher vapor pressure).

Since OHP operation depends on the dominance of surface tension forces for ensuring capillary flow, the magnitude and direction of gravity will, in general, affect OHP thermal performance [14,18,25,64,65,71–73]. For terrestrial gravity environments (i.e. 1*g*), this dependence is often demonstrated experimentally by altering the OHP's operating orientation and relative positioning of its evaporator and condenser. An OHP in the vertical bottom-heating orientation (or 'mode') is descriptive of it being collinear with the gravity vector and its condenser above its evaporator; while an OHP in the horizontal orientation indicates that the OHP is perpendicular to the gravity vector. Riehl demonstrated that, for a constant fill ratio of 50%, the sensitivity of an OHP's thermal performance to working fluid is exaggerated when the OHP is operating in the horizontal orientation [74]. This was demonstrated for a variety of working fluids, including: water, methanol, acetone, isopropyl alcohol, and ethanol. Variation of the OHP's effective thermal conductivity was found to vary by ± 19% when changing working fluids with the OHP in the bottom-heating mode, while the variation was ± 53% in the horizontal orientation.

To combat adverse gravity effects, for a given working fluid, one can alter the OHP structure and design, by, for example: increasing the number of turns [24], decreasing the channel diameter [19], using check-valves [75] and/or increasing the number of channel layers [24,76,77]. The number of channel layers is of interest for high heat flux thermal management, as well as gravity combatting, since this allows the OHP

structure to overlap itself, thus becoming denser. Traditional OHP designs consist of a channel structure that remains in one plane, while multi-layered OHPs (ML-OHPs) consist of a channel that meanders through multiple planes. By having a multi-directional channel structure, the ML-OHP can be less prone to gravity force and provide for a wider range of heating/cooling boundary conditions [24].

Thompson et al. experimentally investigated a copper, flat-plate ML-OHP (two layers) filled with either water or acetone [75,76]. In addition to varying the working fluid and orientation, the heating area, and thus OHP evaporator size, was varied. It was demonstrated that increasing the OHP channel layer number could allow for higher heat flux mitigation (i.e. ~ 300 W/cm^2 was observed) and an increased range of operating orientations in which thermal performance is not altered. The orientation-dependence of the ML-OHP was shown to become stronger as the heating area was reduced, and this suggests that the OHP design investigated may have not been entirely optimal. Borgemeyer et al. experimentally investigated a tubular ML-OHP (two layers) filled 50% with water and observed exceptional thermal performance (~400 W capability) which was attributed to the OHP multi-layer design [78]. The evaporator-to-condenser temperature difference was found to decrease as power input increased. Smoot and Ma investigated the effect of channel layer number (up to three) and operating orientation on the thermal performance of a 229 x 76 x 13 mm^3 copper ML-OHP [77]. The device consisted of a single-layer OHP brazed between a double-layer, interconnected OHP; creating two independent closed-loop structures that were either partially filled with water (at 50%) or remained empty. The results demonstrated that the utilization of more channel layers can significantly increase the OHP heat transfer capability (i.e. ~ 8 kW). It

was further confirmed that the utilization of an ML-OHP with interconnected channels between layers provides for less sensitivity to operating orientation. In contrast, a ML-OHP with independent/stacked single-plane channel circuits is more prone to operating orientation limitations, but can have a reduced start-up power requirement.

To date, ML-OHPs have been fabricated using traditional manufacturing methods, in which mini-channels are milled/etched and then cover plates are either mechanically or metallurgically (*e.g.* furnace brazing) attached for sealing purposes. While these methods are proven means for manufacturing single- or double-layer OHPs, the fabrication of a ML-OHP with interconnected channels exceeding two layers is challenging; especially while maintaining hermetic-grade channel encapsulation. The geometry and complexity of the OHP channel structure is also severely constrained by manufacturing capability, available resources and time. Although ultrasonic consolidation (UC) has been demonstrated as a successful means for fabricating aluminum OHPs [79], its utility for realizing highly-complex ML-OHPs and other types of TGPs remains at question.

Additive manufacturing (AM) is an appealing method for generating complex, metallic components from the ground-up directly from computer-sourced solid models (i.e. CAD). For metals, AM is commonly accomplished by the repetitious melting and solidification of metallic powder via directed energy in the form of a laser or electron beam. One common technique for the AM of metals is Laser Powder Bed Fusion (L-PBF) [80]. During L-PBF, successive solid layers of a part are formed by uniformly distributing and selectively fusing (via a laser) a bed of metallic powder under an inert protective atmosphere.

The use of L-PBF for generating application-tailored components is currently being realized in the biomedical and aerospace industries [81,82]. Structures with high degrees of geometric complexity are readily manufacturable, as un-melted particles within the L-PBF powder bed structurally support subsequent layers during their deposition; allowing for the fabrication of internal features and channels. With regard to OHPs, L-PBF provides new design options for channel geometry, number of channel layers, working material (i.e. materials other than copper or aluminum), surface features, alternate hermetic sealing methods and more. As an illustrative example, L-PBF allows one to construct an OHP with six layers of triangular channels parallel to various, tilted planes. With regard to fabricating surface-mounted heat sinks for electronics cooling, AM also provides a unique opportunity to manufacture heat transfer devices with better-matching CTEs and higher melting temperatures. Although various AM methods have been proven successful in building Ti-6Al-4V components worthy for application, the mechanical integrity of such components is still relatively unknown and this is important when considering their use in high pressure or high thermal/mechanical cycling applications [83–86].

In this study, a novel high-temperature, CTE-matching material desirable for many applications – Ti-6Al-4V – is utilized for fabricating a ML-OHP with four interconnected layers of circular mini-channels via L-PBF. The ML-OHP design and manufacture are discussed and then followed by details of the experimental setup and procedure. Results demonstrating the thermal performance of the ML-OHP, as well as its internal channel surface condition, are then provided.

4.2 Prototype Design and Manufacturing

A titanium alloy (Ti-6Al-4V) ML-OHP, shown in Figure 4.1, was manufactured layer-by-layer atop a 10 x 10 x 1 cm^3 titanium platen within an argon purged L-PBF system (ProX 100™) equipped with a 50 W fiber laser [87]. Gas atomized Ti-6Al-4V spherical particles (ASTM B347 Grade 5), with a diameter range of 15-45 μm, were utilized in their as-received condition. The 50.80 x 38.10 x 15.75 mm^3 ML-OHP consisted of four interconnected, horizontal layers of circular mini-channels – forming one closed, continuous loop. Using Equation 4.1, the channel diameter was selected as Ø ≅ 1.52 mm to ensure capillarity of the multiple working fluids investigated. Ti-6Al-4V was chosen for the manufacture of the ML-OHP due to its proven additive-manufacturability and thermal expansion properties, i.e. CTE. Unlike the CTEs of traditional heat transfer materials such as copper (~17 x 10^{-6} K^{-1}) and aluminum (~23 x 10^{-6} K^{-1}), Ti-6Al-4V has a CTE (~9 x 10^{-6} K^{-1}) closer in magnitude to that of silicon (~3 x 10^{-6} K^{-1}), a common semiconductor material used in integrated circuits.

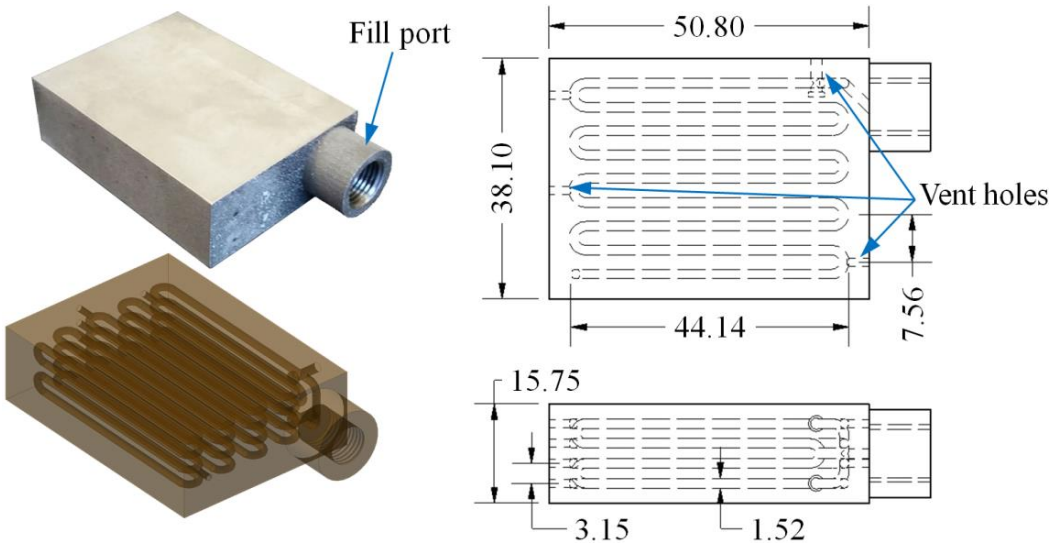

Figure 4.1 Ti-6Al-4V ML-OHP with fill port and vent holes: (left) photograph after milling of faces with transparent CAD part and (right) dimensioned drawings (in millimeters).

Manufacturer-suggested process parameters for Ti-6Al-4V were employed to fabricate the ML-OHP with minimal porosity, including a laser power and scanning speed of 49 W and 40 cm/s, respectively. The nominal powder layer thickness and hatch distance (distance between adjacent laser passes within the same layer) used during fabrication were 70 µm and 30 µm, respectively. The ML-OHP was built vertically upward; with the majority of its channel structure perpendicular to the build plate. Parallel laser scans were performed at 45º angles while depositing each new layer of material. After fabrication, the ML-OHP was sheared off the build plate using electrical discharge machining (EDM).

Parts fabricated via L-PBF are prone to possessing relatively rough surfaces due to powder size variation, partially melted powder remaining at the edges, and potential balling phenomena at the trailing melt pool. Hence, the as-built ML-OHP had two of its sides faced (via end-milling) to obtain smoother surfaces for better contact with

heating/cooling blocks during experimentation. A photograph of the post-PBF, machined ML-OHP is provided in Figure 4.1. The encapsulated, un-melted powder within the closed-loop channel structure was sought for removal via a de-powdering process; hence, nine vent holes (two at Ø 1.83 mm and seven at Ø 1.27 mm) were drilled (and tapped) into the sides of ML-OHP channel layers. Powder was forced out of the ML-OHP, layer-by-layer, by supplying pressurized air (~1 MPa) through the vent holes. After de-powdering each layer, the vent holes were sealed using titanium screws (0-80 UNF or 2-56 UNC threaded plugs), which were secured in place with thread locker (Loctite® 222). The fill port (Ø 3.18 mm, 1/8 NPT), protruding from the side of the ML-OHP as shown in Figure 4.1, was tapped and a vacuum-grade fitting (Swagelok® SS-1-UT-1-2) was installed.

A phosphorous-deoxidized copper (alloy 122) tube (0.8 mm ID) was connected to the fill port, and the ML-OHP was connected in-line with a vacuum pump (Fisher Scientific Maxima C Plus Model M8C) assembly. The ML-OHP internal channel structure was repetitiously flushed with acetone (99.5% purity) for removal of excess powder and oxide. Prior to the introduction of the working fluid, the fitted ML-OHP assembly was confirmed to hold a vacuum for a prolonged period of time by monitoring the pressure (MKS INC 910 pressure transducer, ± 5% accuracy) of the vacuum pump/heat pipe assembly. To investigate the effects of working fluid, approximately 70% (± 2%) of the heat pipe channel was filled with either: high performance liquid chromatography (HPLC)-grade water (Fisher Scientific W5SK-4, 1 g/mL density, 100% purity), HPLC-grade acetone (Fisher Scientific A949-4, 0.7857 g/mL density, 99.5% purity), n-pentane (Aqua Solutions P1033-4L, 0.63 g/mL density, 99% purity) or

Novec^{TM} 7200 (3M, 1.43 g/mL density, standard purity). All working fluids were de-gassed and 'back-filled' into the evacuated ML-OHP (~3 Pa vacuum) to prevent air from adversely affecting its thermal performance. After filling the ML-OHP, its charging tube was pneumatically crimped to ensure a hermetic seal.

4.3 Experimental Setup and Procedure

The ML-OHP was experimentally characterized for thermal performance using a setup shown schematically in Figure 4.2. In order to determine the effects of gravity, the device was suspended in an insulated, rotatable test frame for accomplishing horizontal (i.e. parallel to ground), vertical bottom-heating and vertical top-heating orientations. As shown in Figure 4.2, the ML-OHP evaporator and condenser were located on opposing faces and sides. This heating/cooling configuration was selected for maximizing the layer-wise heat flux (i.e. along the OHP thickness). The evaporator and condenser areas were approximately equal; each accounting for ~ 25.4 x 38.1 mm² (or about half) of the machined face area.

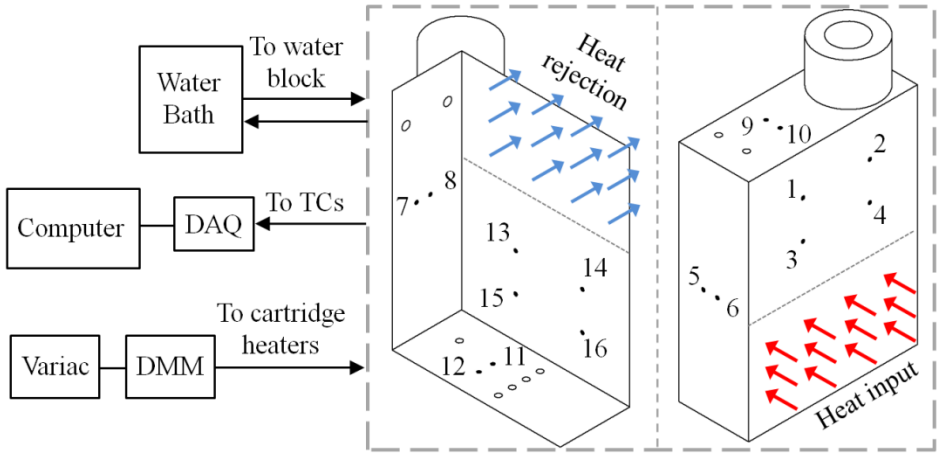

Figure 4.2 Experimental setup and thermocouple (TC) locations (black dots) along the bottom-heated ML-OHP surface.

An aluminum water block (with two Ø 10 mm channels) was tightly clamped to the ML-OHP condenser area and connected to a temperature-controlled water bath/circulator (PolyScience AD15R-30-A11B) to allow for an inlet water temperature of approximately 20 ºC at 20.1 l/min flowrate. An aluminum hot plate - consisting of two embedded 150 W cartridge heaters (Watlow) - was clamped to the ML-OHP evaporator for achieving near-uniform heat flux conditions. A Variac and digital multimeter (DMM) were utilized for controlling the power supplied to the cartridge heaters, which was estimated by $P = V^2/R$ (where R is the heater resitance). Sixteen type-T thermocouples (Omega) were fixed (via Loctite® 495) on the surface of the ML-OHP with locations shown in Figure 4.2. Temperature measurements were collected using a data acquisition (DAQ) system (National Instruments cDAQ-9178 chassis with NI-9213 temperature module) connected to a computer equipped with Lab View Signal Express.

Power was supplied to the cartridge heaters in 5 W increments from 5 to 50 W (+/- 0.5 W) or until the maximum temperature of the ML-OHP reached ~150 ºC. After introducing a new power input, the ML-OHP surface temperature field was allowed to respond until a (pseudo) steady-state was achieved – as evidenced by temperatures oscillating with a time-invariant mean. This steady-state temperature field was recorded for approximately 3 minutes. This process was repeated for each working fluid and orientation investigated (vertical bottom heating and horizontal). The ML-OHP, while filled with each working fluid, was also tested in an 'inverted', vertical top-heating orientation at a power input of approximately 50 W. Thermal paste/epoxy (Omegatherm 201) was applied to condenser and evaporator surfaces, as well as around cartridge heaters, to reduce thermal contact resistance. The ML-OHP, while clamped against the

hot plate and water block, was well insulated on all sides while suspended in the rotatable test frame. Heat loss to the environment during testing was found to increase with power input but was less than 5% at the highest power input (50 W). The ML-OHP was also tested while empty (and open to atmosphere) for establishing a baseline performance curve.

The average, steady-state temperature difference between the ML-OHP evaporator and condenser, ΔT_{avg}, was calculated using time-averaged temperature measurements at the j^{th} location identified in Figure 4.2, i.e. T_j, via Equation 4.2:

$$\Delta T_{\text{avg}} = \left(\frac{T_{11}+T_{12}+T_{14}+T_{15}}{4}\right) - \left(\frac{T_1+T_2+T_9+T_{10}}{4}\right) \tag{4.2}$$

These measurement locations were selected to account for temperature gradients along the channel-wise and layer-wise directions in the evaporator and condenser. The temperature difference provided in Equation 4.2 was used for defining an effective OHP thermal resistance, ψ_{eff}, for a specific power input, P, i.e.

$$\psi_{\text{eff}} = \frac{\Delta T_{\text{avg}}}{P} \tag{4.3}$$

Since the heat transfer through the OHP is less than the power input, the exact OHP thermal resistance, which is per unit heat transfer, will be higher. The metrics defined in Equations 4.2 - 4.3 were used for quantifying the thermal performance of the ML-OHP during its operation while using various working fluids (water, acetone, Novec 7200, n-pentane, air/empty), working orientations (vertical bottom-heating, horizontal, vertical top-heating) and power inputs (5-50 W).

The error in the supplied voltage, cartridge heaters resistance, and ΔT_{avg} was constant at ±0.2 V, ±0.1 Ω, and ±0.5 ºC, respectively. Thus the uncertainty of ψ_{eff} varied

with power input as V increased. The error was largest at lower power inputs when the voltage and temperature uncertainty was large compared to the magnitude and the respective variables. In general, the error for ψ_{eff} ranged from +10%/-11% at 5 W to +8%/+2% at 50 W. The asymmetric uncertainty is due to the ML-OHP heat loss, which is always negative.

To aid discussion regarding the effects of working fluid properties on ML-OHP thermal performance, select dimensionless parameter groups were employed, including the Bond number (Bo), Prandtl number (Pr), inverse Jakob number (Ja^{-1}), Galilei number (Ga), and Laplace number (La). Working fluid properties, as summarized in Table 4.1, were evaluated at a nominal ML-OHP operating temperature of 50 ºC, saturation pressure, standard acceleration due to gravity (g = 9.81 m/s²), and a reference temperature difference (ΔT_o) of 20 ºC. The internal channel surface possessed roughness approximately half of the powder diameter (to be discussed); thus, an effective internal channel radius as $r_H \cong 730$ μm, was utilized as the characteristic length. Property values listed in Table 4.1 were utilized for evaluating the chosen dimensionless groups and their corresponding formulae and magnitudes are summarized in Table 4.2.

Table 4.1 Thermophysical and rheological properties of investigated working fluids at 50 ºC and saturation pressure.

	ρ_l (kg/m^3)	ρ_v (kg/m^3)	σ (N/m)	h_{lv} (kJ/kg)	k_l (W/m·K)	$c_{p,l}$ (kJ/kg·K)	μ_l (μPa·s)
water [88]	988	0.083	0.068	2382	0.644	4.19	547
Novec 7200 [89,90]	1365	4.47	0.011	119	0.068	1.2	468
acetone [91,92]	757	1.71	0.02	525	0.172	2.25	250
n-pentane [88]	595	4.55	0.013	346	0.10	2.44	177

Table 4.2 Non-dimensional numbers for investigated working fluids and ML-OHP using property values from Table 4.1, a characteristic length of rH, standard acceleration due to gravity, g = 9.81 m/s², and reference temperature difference (ΔT_o) of 20 ºC.

	Bond number (Bo)	**Prandtl number (Pr)**	**Inverse Jakob number (Ja^{-1})**	**Galilei number (Ga)**	**Laplace number (La)**
	$\frac{r_H^2 g(\rho_l - \rho_v)}{\sigma}$	$\frac{C_{p,l}\mu_l}{k_l}$	$\frac{h_{lv}}{C_{p,l}\Delta T_o}$	$\frac{g r_H^3 \rho_l^2}{\mu_l^2}$	$\frac{\sigma \rho_l r_H}{\mu_l^2}$
Water	0.08	3.6	28.4	12,450	163,913
Novec 7200	0.65	8.3	5.0	32,465	50,045
acetone	0.20	3.3	11.7	34,990	176,835
n-pentane	0.24	4.3	7.1	43,125	180,234

Bo	gravitational forces / surface tension forces
Pr	momentum diffusivity / thermal diffusivity
Ja^{-1}	latent energy absorbed / sensible energy absorbed (liquid-vapor phase change at ΔT_o)
Ga	gravitational forces / viscous forces
La	surface tension / momentum diffusivity

4.4 Experimental Results

4.4.1 Channel Surface Quality Inspection

Parts fabricated via PBF can have residual, partially-melted particles sintered along their free surfaces within or along the periphery of the part. Although external surfaces of PBF parts can be readily machined for reducing surface roughness, internal surfaces (especially with capillary dimension) are more challenging to post process. Hence, the internal surface quality and topology of the ML-OHP channel structure is worth investigating, as such features can generally impact a fluid's wetting/wicking behavior and heat transfer in an OHP [93–95]. For instance, the thin film evaporation, a dominant heat transfer mechanism in the OHP evaporator, as well as the fluid pulsation and convection/condensation, throughout the OHP, depend on the fluid-to-wall wetting behavior (e.g. contact angle, meniscus formation) which depends on surface roughness and condition of the channels. The sensible heat transfer between the evaporator and condenser, accomplished via oscillating advection of the liquid, is also affected by the wall surface roughness as this impacts the channel structure pressure drop, and thus the resulting flow behavior.

The channel surface quality inside the ML-OHP was first inspected via neutron radiography, which is a unique, non-destructive means for visualizing features within various materials/media. In this method, neutrons are ejected from a neutron source and aimed toward the to-be-inspected materials positioned in front of a camera/detector [96]. The amount of neutrons that pass through or are absorbed by the material depend on the material type, size and density. The High Flux Isotope Reactor (HFIR) CG-1D neutron imaging facilities at Oak Ridge National Laboratory [97,98] were utilized. The ML-OHP

was positioned in front of a charge-coupled device (CCD) camera in line with a neutron beam. The detector collected images at a resolution of 100 micron at a rate of 1 fps. Radiographs were produced by sampling over a 50 s time frame. The ML-OHP was inspected as-is; free of any heating or cooling, and its orientation was varied in between runs to obtain frontal and side views of the channel structure. Prior to inspection, the ML-OHP was attached to a vacuum/charging station for removal of its internal working fluid; which was known to be water. Since the goal of the visualization was to obtain qualitative data, neutron radiographs were only bright field corrected; no special attention was given to volumetric measurements via pixel intensity correlation. The time-averaged (over 50 s), contrast-adjusted neutron radiographs of the ML-OHP's front and side are shown in Figure 4.3a, and Figure 4.3b, respectively. Note that the channel structure appears brighter in Figure 4.3b due to there being less solid material attenuating in that orientation, and the Ti-6Al-4V material appears more transparent (attenuates less) than the residual water due its atomic composition.

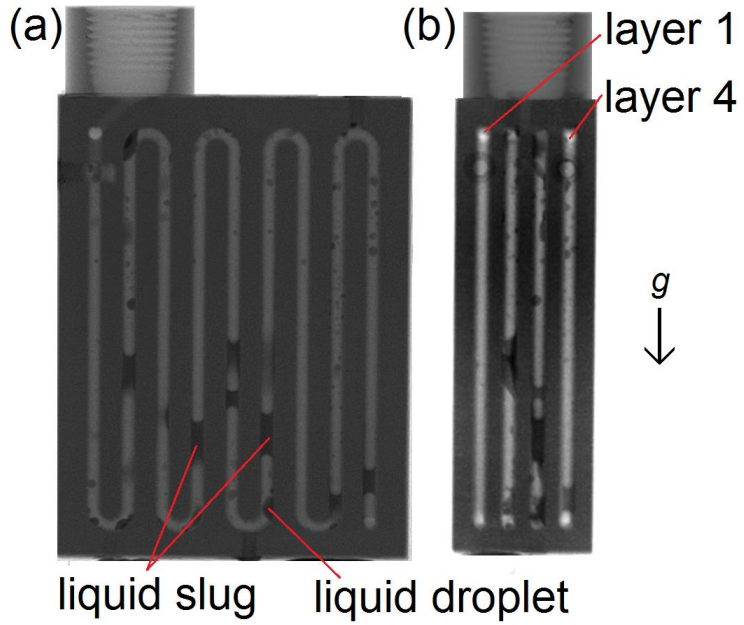

Figure 4.3 Neutron radiographs of ML-OHP with residual water slugs and droplets a) front and b) side view

As evidenced in the neutron radiographs shown in Figure 4.3, volumes of remnant water existed unevenly along the internal channel structure, despite the preliminary vacuuming procedure. This water most likely remained in the ML-OHP due to its (i) relatively high surface tension and the (ii) notable pressure drop across the entire ML-OHP channel structure. The trapped water slugs exhibit concave menisci indicating secondary wicking along the capillary channel walls. Smaller volumes of residual water, in the form of speckles or droplets, are also observed, further indicating the wicking and adhesive properties of the sintered walls. This is of interest, since previous neutron visualization experiments on liquid wetting behavior in relatively smoother OHP structures [16,17] demonstrate full channel wicking with no major evidence of isolated speckles/droplets along walls. Most water slugs/droplets are seen in the lower portions of the ML-OHP, indicating the influence of gravity. Figure 4.3 further indicates that the

ML-OHP internal channel structure was clear of any major, solid-phase blockages or other channel obstructions, and this indicates that the OHP was genuinely closed-loop and that the PBF and de-powdering processes were both effective in maintaining channel cross-section continuity.

Via EDM, a previously-manufactured ML-OHP prototype was sectioned to allow portions of the channel structure to be examined using a field emission scanning electron microscope (FESEM). The channel roughness is clearly observable in Figure 4.4a; especially by comparing it to the EDM'ed surface visible along the top edge of the image. Figure 4.4b better shows the details of the Ti-6Al-4V particles closer to the channel wall and the spherical morphology of the employed powder is confirmed. The majority of sintered particles were found to conform to the manufacturer-specified powder size (15-45 μm), although some outliers are evident in Figure 4.4b. For the arbitrarily-selected regions of the channel structure inspected via FESEM, no major differences in wall topology was observed and the sections shown in Figure 4.4 are deemed representative.

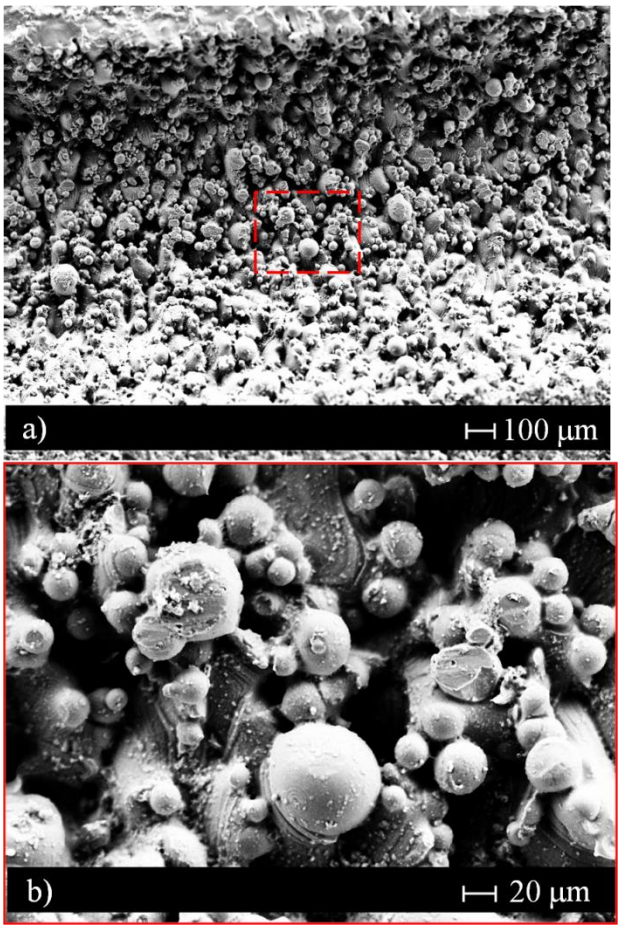

Figure 4.4 FESEM images of a channel surface at (a) 54x and (b) 310x magnification

The benefit/cost of having PBF-sourced, sintered channel structures within an OHP, or any other heat transfer device, will depend on its operating conditions/application. For the case of OHPs, the roughened surfaces can decrease the start-up power threshold of the OHP (due to boiling enhancements and secondary capillary action) while decreasing its power limit (since pressure balancing within the evaporator becomes easier to obtain during operation) [94,95,99,100]. However, if these characteristics were not needed or even undesirable for a certain application, methods such as purging the channels with an acidic solution to etch the sintered particles could be an option for reducing channel roughness. Residual powder not attached to channel could prove advantageous for OHP

operation, as low-concentration, micro/nano-fluid suspensions can form due to mixing from consistent fluid pulsation along the channel structure.

4.4.2 Steady State Temperature Oscillations

The Ti-6Al-4V ML-OHP was found to operate successfully for all experimental conditions investigated after a critical power input, which ranged between 10 – 25 W, was achieved. In most cases, the ML-OHP surface temperature field oscillated, indicating cyclic phase-change heat transfer and fluid pulsation within its channel structure. Representative ML-OHP steady-state temperature oscillations, at the T_{14} evaporator-side location (see Figure 4.2), for a 50 W power input, and for various orientations and working fluids, are shown in Figure 4.5. The ML-OHP was considered to be at steady-state when the long time-scale temperature means became steady, i.e. temperature oscillations about a constant value. Fluids providing for the highest to lowest evaporator temperature (i.e. T_{14} measurement) were: acetone, n-pentane, Novec 7200 and water, respectively, and this remained consistent for all operating orientations investigated. These results suggest that fluids with a low product of Ga and La numbers, i.e. $\sim \rho_L^3/\mu_L^4$, are desirable for minimizing the evaporator operating temperatures. In general, the average ML-OHP evaporator temperature was found to be relatively insensitive, ~2-3% change, to operating orientation. The fact that the ML-OHP still functioned while in the top-heating orientation is a significant demonstration of gravity independence as compared to other types of OHPs possessing less channel layers. The enhanced capillarity of the internal channel structure, due to the peripheral, secondary wicking structure consisting of sintered particles, provides a means to increase liquid pumping

from the condenser to the evaporator. The partially melted powder can increase the capillary pressure inside the OHP, thus reducing gravity effects on fluid flow.

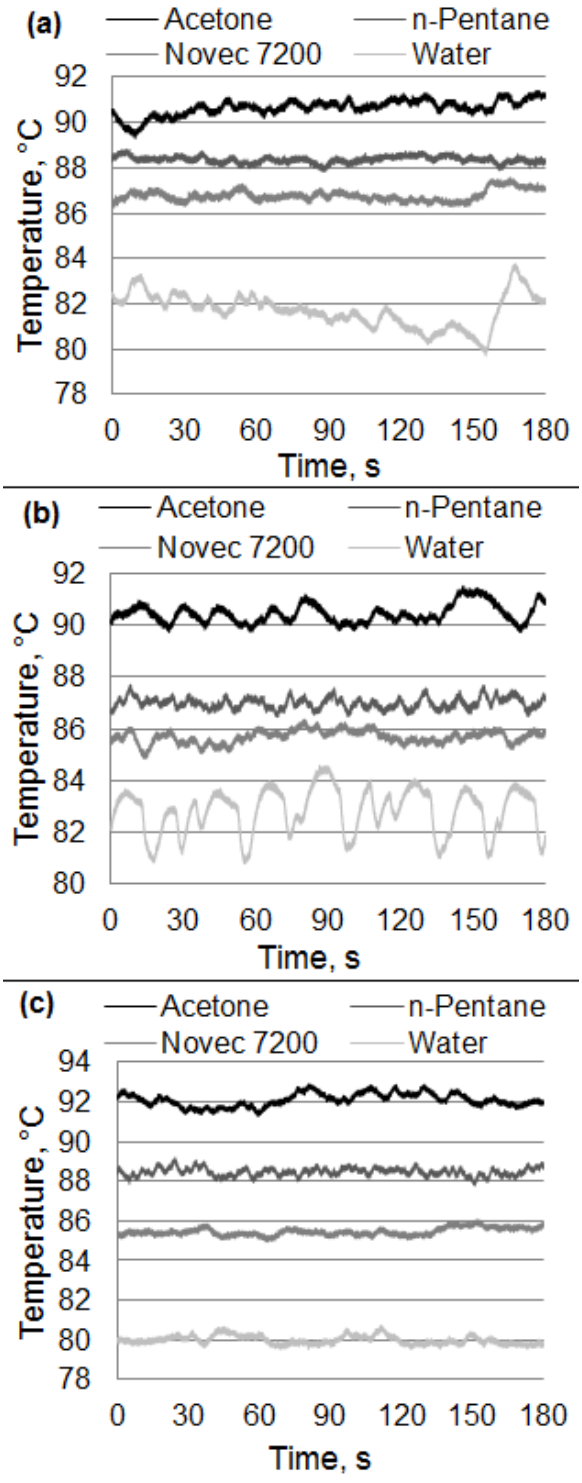

Figure 4.5 Local steady-state ML-OHP surface temperature (T14) vs. time while filled with either acetone, n-pentane, water, or Novec 7200 and operating at P ≅ 50 W for the following heating modes: (a) vertical bottom-heating, (b) vertical top-heating, (c) horizontal.

Although the average T_{14} evaporator temperature remained near constant, the apparent amplitude and frequency of T_{14} were found to depend on the working fluid and the ML-OHP operating orientation. Evaporator temperatures slightly increased for all working fluids in the horizontal orientation, except for water and Novec 7200, which decreased and remained un-changed, respectively. The water ML-OHP was most sensitive to operating orientation, as its T_{14} temperature oscillations changed significantly in both frequency and amplitude for different working orientations. Water temperature oscillations possessed higher apparent frequency while the ML-OHP operated during bottom-heating relative to horizontal and top-heating orientations. Going from vertical bottom-heating to vertical top-heating resulted in the water ML-OHP evaporator temperature field to pulsate at higher amplitude and frequency. This trend was also observed for the other working fluids, but not to the same extent as water. In the horizontal heating mode, the evaporator temperature of the water ML-OHP became more stable, indicating its strong coupling with gravity.

Non-dimensional parameter groups are useful for describing working fluid wetting behavior, capillarity, heat transfer ability, rheology and more. Results suggest that a fluid's Ga number is indicative of its fluid pulsation behavior with respect to gravity. Water, having the lowest Ga and Bo numbers of the group, was highly sensitive to operating orientation, while n-pentane, having the highest Ga number of the group, provided for temperature oscillations near-independent of operating orientation. Working fluids with a high inverted Ja number were observed to provide for higher temperature amplitudes at lower frequency. This is especially evidenced by the water and acetone temperature oscillations during vertical top-heating of the ML-OHP. Based on these

observations, it appears that the working fluid's latent heat of vaporization affects OHP surface temperature oscillation and frequency while also making the OHP more sensitive to operating orientation. Both Novec 7200 and n-pentane have the highest Bo number and appear to provide for the most consistent temperature oscillations irrespective of operating orientation. Acetone and n-pentane have similar temperature oscillations during the horizontal operating mode, and they both share a high La number – indicating the importance of viscosity and surface tension in the absence of direct gravity influence. Both Novec 7200 and n-pentane ML-OHPs had local evaporator temperatures decrease when going from bottom-heating to top-heating orientations, although their thermal resistances increases. It is interesting to note that both of these fluids possess relatively dense vapor and low inverted Ja numbers.

The surface temperature field measured along the ML-OHP was inspected to determine the effect of multiple channel layers on the evaporator-to-condenser heat transfer. The steady-state temperature oscillations as recorded at locations T_1 - T_{15} for the bottom-heated acetone and water ML-OHPs, at ~40 W power input, are provided in Figure 4.6-4.7. Based on the thermocouple arrangement set forth herein (as shown in Figure 4.2), four regions are of concern, including the layer immediately underneath the heat source, i.e. the primary 'evaporator layer', the layer in contact with the heat sink, i.e. the primary 'condenser layer', one of the adiabatic sides of the ML-OHP, as well as the opposite heated/cooled ends of the ML-OHP. In general, the water ML-OHP surface temperature field was substantially more 'active' for all locations measured, suggesting that low Bo and Ga numbers are important in establishing spatially-uniform fluid pulsation with respect to ML-OHP channel layer and region. Such uniform, and strong,

surface pulsations were only observed for the water ML-OHP. All other ML-OHPs demonstrated strong temperature oscillations near the evaporator, but less active oscillations along the ML-OHP sides and near the condenser. Assuming temperature amplitudes are related to latent heat transfer, as the current results suggest; then clearly the high inverse Jakob number of water allows for more severe temperature amplitudes measured along the outer ML-OHP structure. Results indicate that working fluids with lower Pr numbers provide for temperature oscillations of more similar magnitude between the evaporator- and condenser-side regions. For the case of Novec 7200, which has the highest Pr number, the phase-change heat transfer in the condenser is shown to be most likely less than ; occurring in the evaporator.

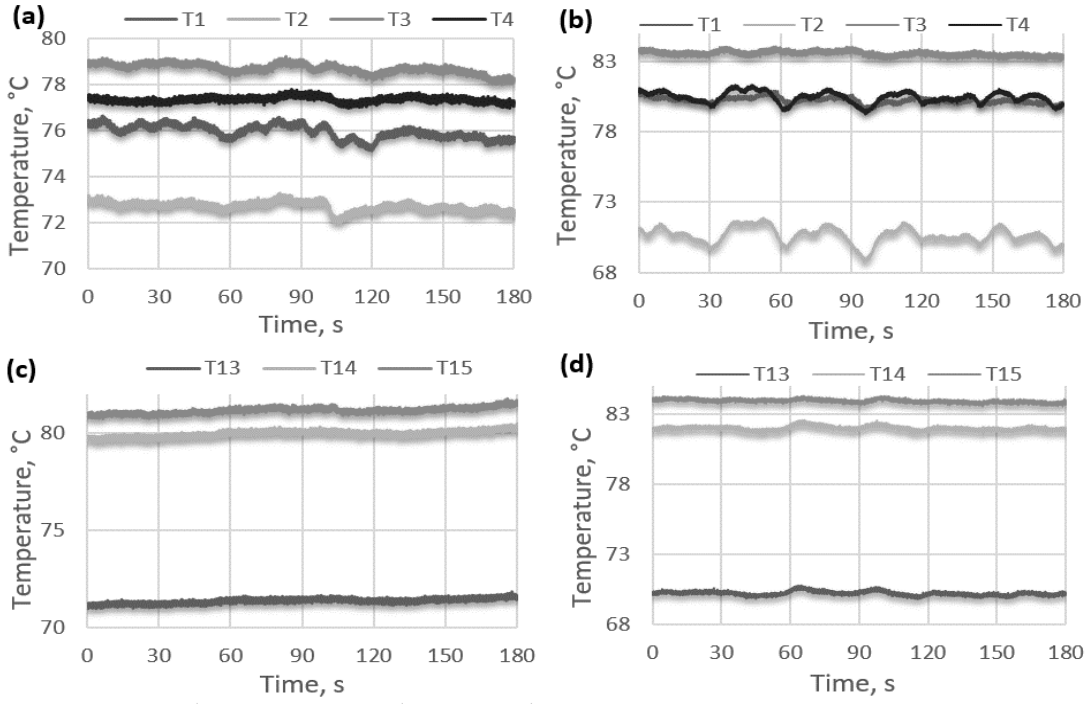

Figure 4.6 Local steady-state ML-OHP surface temperature vs. time at P ≅ 40 W for vertical bottom-heating: (a) acetone 'evaporator layer' T1 - T4, (b) water 'evaporator layer' T1 - T4, (c) acetone 'condenser layer' T13 – T15, (d) water 'condenser layer' T13 – T15.

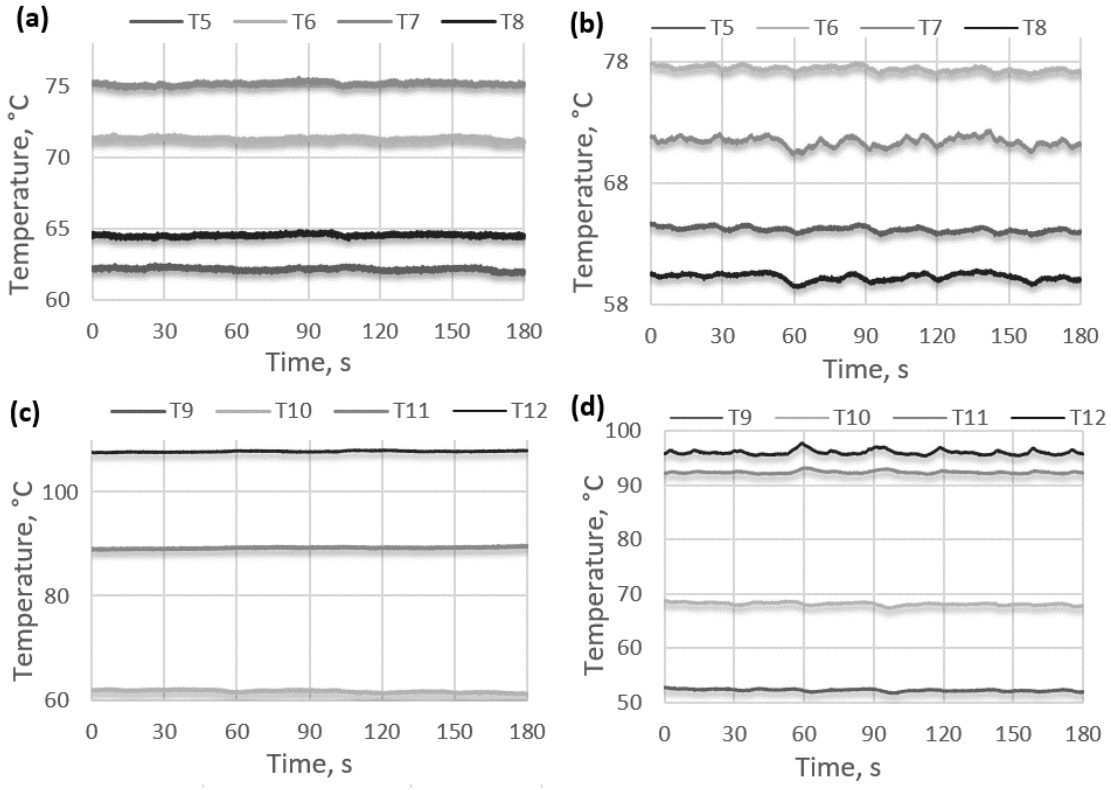

Figure 4.7 Local steady-state ML-OHP surface temperature vs. time at P ≅ 40 W for vertical bottom-heating: (a) acetone 'adiabatic side' T5 – T8, (b) water 'adiabatic side' T5 – T8, (c) acetone evaporator T11 – T12 and condenser T9 – T10 ends, (d) water evaporator T11 – T12 and condenser T9 – T10 ends.

The multi-layer design feature of the ML-OHP allows for higher channel-to-volume density and thus more high heat flux mitigation. Even for the current prototype, in which the channel layer-to-layer (and even adjacent channel-to-channel) distance was not minimized, the evaporator-to-condenser heat flux was found to provide sufficient vapor pressure for fluid pulsation within each of the OHP's four layers; regardless of working fluid used. It is clear that the ML-OHP designer should consider the depth of heat penetration from the heat source, as this will establish the number of heat affected layers capable of producing vapor. Depending on the heat penetration depth and the

heating/cooling configuration, each heat affected layer may behave as an independent OHP. Hence, in order to design the ML-OHP for a given application, it is best to consider the container thermal conductivity, as well as the thermal spreading/constriction resistance, to best estimate the level of heat penetration and number of heat affected layers.

4.4.3 Effective Thermal Resistance

The effective thermal resistance of the ML-OHP for multiple power inputs, during the vertical bottom-heating and horizontal orientations, for all working fluids investigated, is shown in Figure 4.8. It may be seen that the ML-OHP's effective thermal resistance generally decreases as power input increases and that it depends on the working fluid type, operating orientation and power input. The ML-OHP effective thermal resistance, while in the vertical bottom-heating orientation, was found to be lower than that while in the horizontal orientation for most working fluids – demonstrating that the four-layered, closed loop capillary structure is still somewhat gravity dependent. In all cases, the top heating mode proved most detrimental to OHP thermal performance. This was expected, since in these cases the capillary force direction of evaporator-bound condensate is opposite of that for liquid weight. The ML-OHP, while filled with n-pentane or Novec 7200 and operating in the horizontal orientation, started to function near 10 W of power input; and this is ~ 150% lower than that required for water (~25 W) due to its relatively lower viscosity and La number. This also suggests that fluids with relatively high inverted Ja numbers require more heat transfer to initiate their oscillation within an OHP. The acetone ML-OHP in the vertical/bottom-heating orientation had the lowest thermal resistance, and this may be attributed to the low

viscosity and La number of acetone. However, although the effective thermal resistance of the acetone ML-OHP was low, its maximum evaporator temperature was the highest of all fluids investigated as shown in Figure 4.8. The relatively long internal channel structure of the ML-OHP can possess a high pressure drop, and fluids with relatively lower viscosity may be more advantageous for reducing overall thermal resistance.

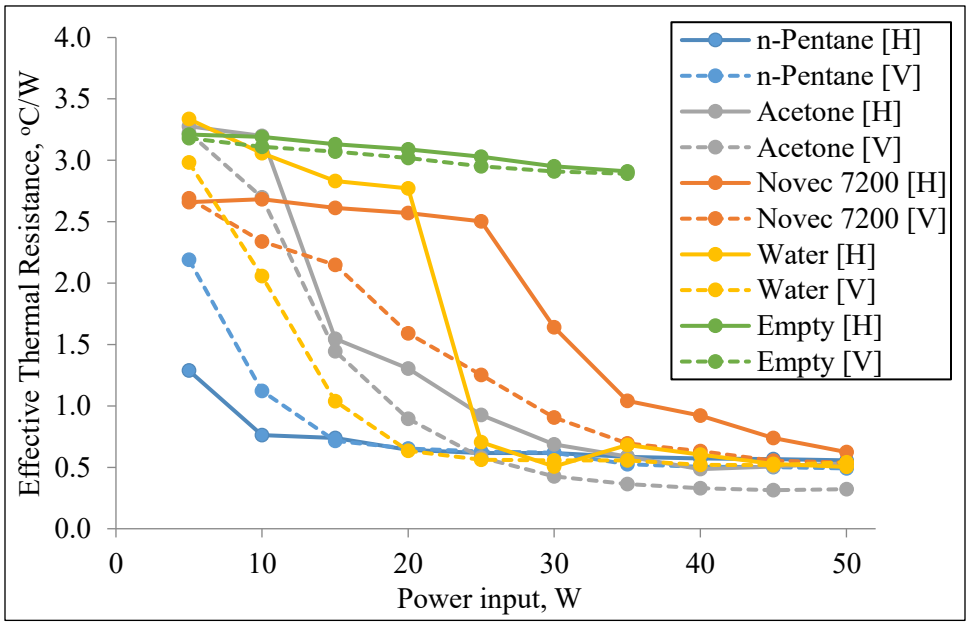

Figure 4.8 Effective ML-OHP thermal resistance vs. power input while filled with either n pentane, water, acetone, Novec 7200 or while empty (control group) in either the vertical (V) or horizontal (H) operating orientation.

As expected, the empty ML-OHP provides for the maximum thermal resistance for all orientations investigated. Relative to the empty ML-OHP, the acetone ML-OHP provides for an 85% lower effective thermal resistance. Without a working fluid to aid thermal transport via phase change and physical oscillations, conduction through the Ti-6Al-4V ML-OHP (a metal with a relatively low thermal conductivity: 6.7 W/m·K) is the only available mode for heat transfer. As shown in Figure 4.9, all ML-OHPs investigated

tend to have an effective thermal resistance that increases going from bottom-heating, to horizontal-heating, then to top-heating. The exception is the water ML-OHP, which performed best while in the horizontal orientation. This indicates that water's unique rheological and inertial properties (providing for relatively low Ga and Bo numbers), combined with the ML-OHP design, provides for a more gravity-dependent ML-OHP. The density of water vapor is also significantly lower than those of the other investigated working fluids and this may also play a role. Water does provide for the lowest effective thermal resistance relative to other fluids while the ML-OHP is in the horizontal orientation; indicating that a low Ja number may be advantageous for optimal OHP operation in absence of a collinear gravity force vector. The results indicate that low La numbers, or high Bo and Pr numbers, may correlate to lower OHP heat transfer ability, as well. This is supported by observing that Novec 7200, which provided for the lowest La, and highest Bo and Pr, for the investigated ML-OHP, resulted in the highest recorded effective thermal resistance for all orientations investigated.

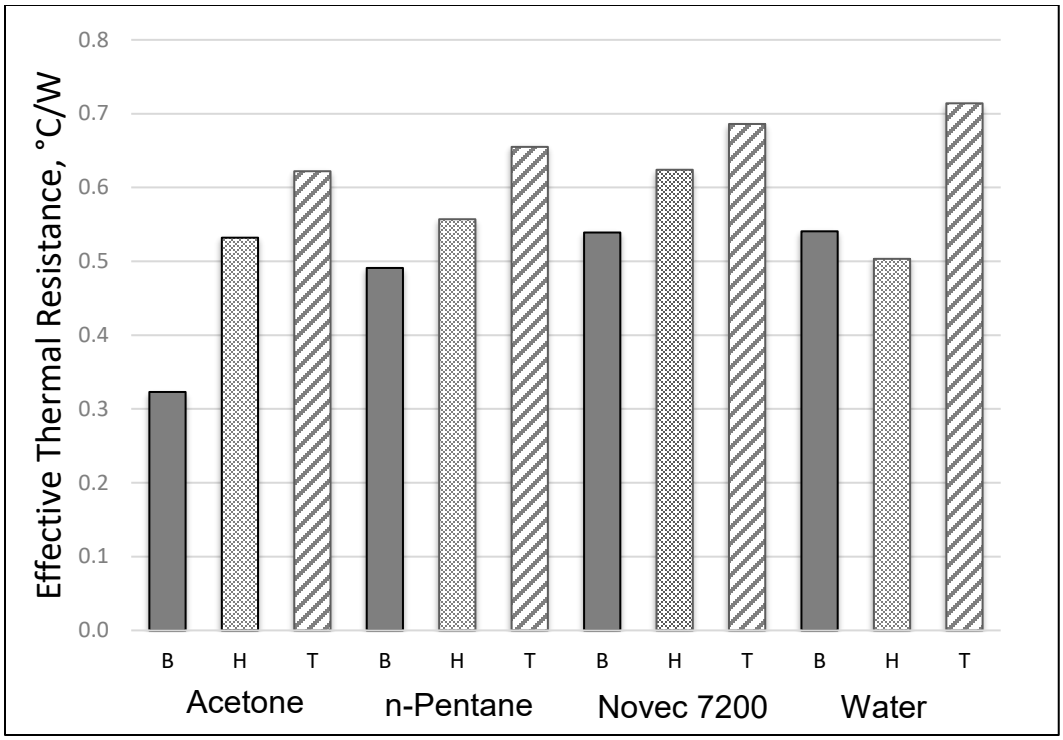

Figure 4.9 Average, effective thermal resistance of ML-OHP while operating at P = 50 W for three different orientations: vertical bottom-heating, 'B', horizontal, 'H', vertical/top-heating, 'T') and various working fluids (water, acetone, n-pentane, Novec 7200).

CHAPTER V

CONCLUSIONS AND FUTURE WORK

5.1 Conclusions

5.1.1 Bent Tube Oscillating Heat Pipe:

A tubular oscillating heat pipe was shaped and tested experimentally at 0°, 45°, and 90° bend angle, with the channels' bend angle placed centrally between the evaporator and condenser. Water, acetone, and n-pentane were used as working fluids to charge BT-OHP and evaluate thermal performance at horizontal and vertical orientations. Power input was varied from 10 to 700 W and the experimental tests were stopped as BT-OHP surface temperature reached 100℃. Some of the major results are summarized below:

1) Bend angle has a significant effect on the performance of the BT-OHP, where the performance of BT-OHP with vertical bottom heating increased as the bend angle increase from 0° to 90°.
2) Working fluid thermal properties have a major effect on the performance of BT-OHP and it depends on the bend angle. Acetone performed better at 0°, while water was superior at 45° and 90° bend angles.
3) Orientation has a direct effect on the thermal performance of BT-OHP as bend angle increase from 0° to 135°, where BT-OHP perform better with vertical bottom heating

orientation for bend angles from 0° to 90° and it performs better with horizontal orientation at 135° bend angle.

4) The best BT-OHP thermal performance occurred at 90° bend angle, vertical bottom heating orientation and using water as a working fluid.

5.1.2 Thermal Connector Oscillating Heat Pipe

A thermal connector oscillating heat pipe (TC-OHP) with L-shape microchannel was machined from a copper plate and tested experimentally as a thermal connector for PCB. The TC-OHP was charged with n-pentane as a working fluid and tested for variable power input from 25 to 250W. The results are summarized below:

1) The TC-OHP performed better than the control under similar conditions, with the thermal performance increasing as the temperature of the PCB increased. The surface temperature of the OHP thermal connector was lower than the control by 16C at 250W.
2) The thermal resistance of TC-OHP thermal connector decreased to be 0.09 W/C as the power input increased.
3) Causal fitting of the thermal connector in the slot with bad contact caused air gaps to be formed, which acted as insulation to reduce the thermal connector performance.

5.1.3 Multi-Layered Flat Plate Oscillating Heat Pipe:

A Ti-6Al-4V multi-layered oscillating heat pipe (ML-OHP) was successfully fabricated using laser powder bed fusion (L-PBF) additive manufacturing. The device consisted of four interconnected layers of circular mini-channels which were successfully de-powdered after L-PBF. The ML-OHP was experimentally investigated in either the

bottom-heating, top-heating, or horizontal orientations, while being partially filled with either Novec 7200, acetone, n-pentane or water. The ML-OHP was heated and cooled on opposing planes and sides to determine heat transfer ability of the stacked layers. The heat pipe was characterized for surface quality, fluid wicking behavior, and thermal performance, and some of the major results are summarized below.

1) Working fluid within the ML-OHP displays unique wicking behavior; due partially to residual, sintered powder along the periphery of the OHP channel. The characteristic surface roughness was found to be almost twice the maximum diameter of the spherical Ti-6Al-4V powder used for manufacture. These features should increase the capillary pumping ability of the OHP and promote boiling heat transfer during start-up, resulting in reduced gravity dependence and a reduced OHP start-up power requirement, respectively.
2) No solid blockages were found within the channel structure, demonstrating the utility of L-PBF for fabricating mini-channel devices. A means for de-powdering the internal channel structure must be integrated at the design phase.
3) The ML-OHP, which consisted of four interconnected channel layers, was shown to operate effectively while filled with water, Novec 7200, acetone or n-pentane, almost independent of operating orientation. This demonstrates that the OHP is 'stackable' when embedded in solid media.
4) The vertically-bottom-heated, acetone ML-OHP and the horizontal-oriented, water ML-OHP each possessed the lowest thermal resistances measured. Working fluids, like n-pentane and Novec 7200, started oscillating at relatively low heat inputs while others,

like water, started oscillating at much higher heat inputs. Novec 7200 provided for the highest effective thermal resistance in all orientations.

5) The ML-OHP evaporator size depends on the number of heat affected layers underneath the heat source and the heating/cooling configuration. Thus, the heat penetration depth resulting from the heat source is of importance, and the thermal spreading resistance of the evaporator and container material should be considered during design.
6) The apparent amplitude and frequency of temperature oscillations were found to depend on working fluid and the ML-OHP operating orientation. The water ML-OHP temperature oscillations were most sensitive, in frequency and amplitude, to operating orientation. The water ML-OHP surface temperature field was the most spatially uniform.
7) Results suggest important trends in non-dimensional numbers, OHP effectiveness and working conditions. Working fluids with low Bond and Prandtl numbers may be more advantageous for effective OHP operation, while higher inverted Jakob numbers appear to correspond to an OHP with larger temperature amplitudes along its external surface. OHPs that employ working fluids with relatively low Galilei numbers may be more prone to adverse gravitational effects, while low Laplace numbers, in the absence of major gravity influence, may be indicative of reduced OHP thermal performance. Fluids with a low Ga x La product may be desirable for minimizing the operating temperature of the OHP.

There are many potential benefits for using emerging AM technology for fabricating state-of-the-art heat transfer devices, especially those with embedded channel

structures. Methods, such as laser-powder bed fusion (L-PBF), are especially beneficial in allowing one to build channel structures with complex cross-sections and arrangements, due to the powder bed serving as an inadvertent support structure during the layer-by-layer manufacturing process. Many metallic powders are available for the thermal engineer to design conformal heat transfer media. For instance, and as demonstrated in this study, one can use Ti-6Al-4V, which has a desirable coefficient of thermal expansion (CTE), for building heat transfer media in intimate contact with silicon-based, heat dissipating sources. The thermal engineers are now challenged with the unique task of 're-designing the wheel'; as once-impossible design concepts are now feasible for manufacture. Since thermal media typically do not experience high mechanical loads during operation, there is less hesitation in introducing additive-manufactured heat exchangers to various applications.

The benefit/cost of having PBF-sourced, partially-sintered channel structures within an OHP, or any other heat transfer device, will depend on its operating conditions/application. For the case of OHPs, the roughened surfaces can decrease the start-up power threshold of the OHP (due to boiling enhancements and secondary capillary action) while decreasing its power limit (since pressure balancing within the evaporator becomes easier to obtain during operation) [12,94,99,100]. However, if these characteristics were not needed or even undesirable for a certain application, methods such as purging the channels with an acidic solution to etch the sintered particles could be an option for reducing channel roughness. Residual powder not attached to channel could prove advantageous for OHP operation, as low-concentration, micro/nano-fluid

suspensions can form due to mixing from consistent fluid pulsation along the channel structure.

5.2 Future Work

The current work has presented three different designs of oscillating heat pipes with different methods of manufacturing. The major potential future works are as follows:

1. Develop a numerical/analytical model on the working fluid inside oscillating heat pipe that considers non-traditional channel structures for a better understanding of the parameters affecting the performance of oscillating heat pipe.

2. Use selective laser melting to manufacture more complex designs of heat pipes and heat exchangers to learn more about advantages and challenges of using this method of manufacturing.

REFERENCES

[1] Moree, G.E., 1965, "Cramming More Components Onto Integrated Circuits," Electronics, 38 (4), PP. 82–85.

[2] Bar-Cohen, A., Maurer, J.J., Felbinger, J.G., 2013, "DARPA's Intra/Interchip Enhanced Cooling (ICECool) Program," CS MANTECH Conf., PP. 171–174.

[3] Bar-Cohen, A., Matin, K., Jankowski, N., Sharar, D., 2015, "Two-Phase Thermal Ground Planes: Technology Development and Parametric Results," ASME J. Electron. Package., 137, PP. 10801.

[4] Zweben, C.H., 2007, "Advances in High-Performance Thermal Management Materials - A Review," J. Adv. Mater. 39, PP. 3–10.

[5] Laun, F.F., Lu, H., Ma, H.B., 2015, "An Experimental Investigation of an Oscillating Heat Pipe Heat Spreader," ASME J. Therm. Sci. Eng. Appl., 7 (6), PP. 21005-1.

[6] Sigurdson, M., Liu, Y., Bozorgi, P., Bothman, D., MacDonald, N., Meinhart, C., 2013, "A large scale Titanium Thermal Ground Plane," Int. J. Heat Mass Transf., 62, PP. 178–183.

[7] Thompson, S.M., Ma, H.B., 2015, "Recent Advances in Two-Phase Thermal Ground Planes," Annu. Rev. Heat Transfer., 18.

[8] Thompson, S.M., Lu, H., Ma, H., 2015, "Thermal Spreading with Flat-Plate Oscillating Heat Pipes," J. Thermophys. Heat Transf., 29, PP. 338–345.

[9] Cai, Q., Chen, B., Tsai, C., 2012, "Design, development and tests of high-performance silicon vapor chamber," J. Micromechanics Microengineering., 22, PP. 35009.

[10] Naphon, P., Wongwises, S., Wiriyasart, S., 2012, "On the thermal cooling of central processing unit of the PCs with vapor chamber," Int. Commun. Heat Mass Transf., 39, PP. 1165–1168.

[11] Boreyko, J.B., Chen, C.H., 2013, "Vapor chambers with jumping-drop liquid return from superhydrophobic condensers," Int. J. Heat Mass Transf., 61, PP. 409–418.

[12] Smoot, C.D., Ma, H.B., 2011, “an Experimental Investigation of Hybrid Oscillating Heat Pipe,” Front. Heat Pipes., 2, PP. 1–6.

[13] Akachi, H., 1990, “Structure of a heat pipe,” U.S. Patent No. 4921041 A.

[14] Ma, H., 2015, “Oscillating Heat Pipes,” Springer.

[15] Akachi, H., Polasek, F., Stulc, P., 1996, “Pulsating Heat Pipes,” 5th Int. Heat Pipe Symp., Melbourne, Australia, pp. 208–217.

[16] Wilson, C., Borgmeyer, B., Winholtz, R. A., Ma, H.B., Jacobson, D.L., Hussey, D.S., Arif, M., 2008, “Visual Observation of Oscillating Heat Pipes Using Neutron Radiography,” J. Thermophys. Heat Transf., 22, PP. 366–372.

[17] Yoon, I., Wilson, C., Borgmeyer, B., Winholtz, R.A., Ma, H.B., Jacobson, D.L., Hussey, D.S., 2012, “Neutron phase volumetry and temperature observations in an oscillating heat pipe,” Int. J. Therm. Sci., 60, PP. 52–60.

[18] Thompson, S.M., Hathaway, A.A., Smoot, C.D., Wilson, C.A., Ma, H.B., Young, R.M., Greenberg, L., Osick, B.R., Van Campen, S., Morgan, B.C., Sharar, D., Jankowski, N., 2011, “Robust Thermal Performance of a Flat-Plate Oscillating Heat Pipe During High-Gravity Loading,” J. Heat Transfer., 133, PP. 104504.

[19] Zhang, Y., Faghri, A., 2008, “Advances and Unsolved Issues in Pulsating Heat Pipes,” Heat Transfer. Eng., 29, PP. 20–44.

[20] Qu, W., Ma, H.B., 2007, “Theoretical analysis of startup of a pulsating heat pipe,” Int. J. Heat Mass Transf., 50, PP. 2309–2316.

[21] Xiao, L., Cao, Y., 2012, “Recent Advances in Pulsating Heat Pipes and Its Derivatives,” J. Enhanc. Heat Transf., 19, PP. 213–231.

[22] Ibrahim, O.T., Monroe, J.G., Thompson, S.M., Shamsaei, N., Bilheux, H., Elwany, A., Bian, L., 2017, “An investigation of a multi-layered oscillating heat pipe additively manufactured from Ti-6Al-4V powder,” Int. J. Heat Mass Transf., 108, PP. 1036–1047.

[23] Khandekar, S., 2004, “Thermo-hydrodynamics of Closed Loop Pulsating Heat Pipes,” Ph.D. dissertation, Universitaet Stuttgart, Germany.

[24] Charoensawan, P., Khandekar, S., Groll, M., Terdtoon, P., 2003, “Closed loop pulsating heat pipes - Part A: Parametric experimental investigations,” Appl. Therm. Eng., 23, PP. 2009–2020.

[25] Gu, J., Kawaji, M., Futamata, R., 2004, “Effects of Gravity on the Performance of Pulsating Heat Pipes,” Journal of Thermodynamics and Heat Transfer, 18.

[26] Sakulchangsatjatai, P., Terdtoon, P., Wongratanaphisan, T., Kamonpet, P., Murakami, M., 2004, "Operation modeling of closed-end and closed-loop oscillating heat pipes at normal operating condition," Appl. Therm. Eng., 24, PP. 995–1008.

[27] Rittidech, S., Terdtoon, P., Murakami, M., Kamonpet, P., Jompakdee, W., 2003, "Correlation to predict heat transfer characteristics of a closed-end oscillating heat pipe at normal operating condition," Appl. Therm. Eng., 23, PP. 497–510.

[28] Charoensawan, P., Terdtoon, P., 2008, "Experimental Investigation of Thermal Performance of Horizontal Closed-Loop Oscillating Heat Pipes," Appl. Therm. Eng., 28, PP. 460–466.

[29] Rittidech, S., Pipatpaiboon, N., Terdtoon, P., 2007, "Heat-transfer characteristics of a closed-loop oscillating heat-pipe with check valves," Appl. Energy., 84, PP. 565–577.

[30] Yang, H., Khandekar, S., Groll, M., 2009, "Performance characteristics of pulsating heat pipes as integral thermal spreaders," Int. J. Therm. Sci., 48, PP. 815–824.

[31] Li, J., Yan, L., 2008, "Experimental research on heat transfer of pulsating heat pipe," J. Therm. Sci., 17, PP. 181–185.

[32] Qu J., Wu H., Cheng P., 2009, "Experiment study on thermal performance of a siliconbased micro pulsating heat pipe" ASME 2nd Int. Conf. on Moicro/Nanoscale Heat and Mass Transfer, 3, PP. 629-634.

[33] Chien, K.H., Lin, Y.T., Chen, Y.R., Yang, K.S., Wang, C.C., 2012, "A novel design of pulsating heat pipe with fewer turns applicable to all orientations," Int. J. Heat Mass Transf., 55, PP. 5722–5728.

[34] Ma, Y., Zhang, H., 2006, "Analysis of Heat Transfer Performance of Oscillating Heat Pipes Based on a Central Composite Design1," Chinese J. Chem. Eng., 14, PP. 223–228.

[35] Yang, H., Khandekar, S., Groll, M., 2008, "Operational limit of closed loop pulsating heat pipes," Appl. Therm. Eng., 28, PP. 49–59.

[36] Gu, J., Kawaji, M., Futamata, R., 2005, "Microgravity performance of micro pulsating heat pipes," Microgravity - Sci. Technol., 16. PP. 181–185.

[37] Taft, B.S., Williams, A.D., Drolen, B.L., 2012, "Review of pulsating heat pipe working fluid selection," Journal of Thermodynamics and Heat Transfer, 26, PP. 651-656.

[38] Melkikh, A. V., Dolgirev, Y.E., 2006, “Self-oscillations in oscillating heat pipes,” High Temp., 44 (7), PP. 542–547.

[39] Rittidech, S., Wannapakne, S., 2007, “Experimental study of the performance of a solar collector by closed-end oscillating heat pipe (CEOHP),” Appl. Therm. Eng., 27, PP. 1978–1985.

[40] Meena, P., Rittidech, S., Poomsa-ad, N., 2007, “Closed-loop oscillating heat-pipe with check valves (CLOHP/CVs) air-preheater for reducing relative humidity in drying systems,” Appl. Energy., 84 (4), PP. 363–373.

[41] Wannapakhe, S., Rittidech, S., Bubphachot, B., Watanabe, O., 2009, “Heat transfer rate of a closed-loop oscillating heat pipe with check valves using silver nanofluid as working fluid,” J. Mech. Sci. Technol., 23 , PP. 1576–1582.

[42] Lin, Y.-H., Kang, S.-W., Chen, H.-L., 2008, “Effect of silver nano-fluid on pulsating heat pipe thermal performance,” Appl. Therm. Eng., 28, PP. 1312–1317.

[43] Maydanik, Y.F., Dmitrin, V.I., Pastukhov, V.G., 2009, “Compact cooler for electronics on the basis of a pulsating heat pipe,” Appl. Therm. Eng., 29, PP. 3511–3517.

[44] Chen, P.-H., Lee, Y.-W., Chang, T.-L., 2009, “Predicting thermal instability in a closed loop pulsating heat pipe system,” Appl. Therm. Eng., 29, PP. 1566–1576.

[45] Lin, Y.-H., Kang, S.-W., Wu, T.-Y., 2009, “Fabrication of polydimethylsiloxane (PDMS) pulsating heat pipe,” Appl. Therm. Eng., 29, PP. 573–580.

[46] Lin, Z., Wang, S., Zhang, W., 2009, “Experimental study on microcapsule fluid oscillating heat pipe,” Sci. China, Ser. E Technol. Sci., 52, PP. 1601–1606.

[47] Demer, F. M., 1959, “Electrical assembly housing” U.S. Patent 2 881 364.

[48] Brown, D. L., Huebner, V. J., 1971, “Industrial control system with means for releasably securing a plurality of electronic modules,” U.S. Patent 3 566 190.

[49] Fedele, D., 1974, “Circuit board anchor having constrained deformable strut,”U.S. Patent 3 845 359.

[50] Prater, E. F., 1976, “Printed circuit board retainer,” U.S. Patent 3 970 198.

[51] Basmajian, F. J., Kurtz, R. C., 1979, “Circuit board clamping assembly,”U.S. Patent 4 157 583.

[52] Johnson, G. R., 1980, “Printed circuit board guide spring,”U.S. Patent 4 214 292.

[53] Wenz, C. F., 1971, “Card module and end wall treatment facilitating heat transfer and sliding,” U.S. Patent 3 631 325.

[54] Pesek, C., 1973, “Circuit board package with wedge shaped covers,”U.S. Patent 3 735 206.

[55] Yousif, A.S., Solbrekken, G.L., 2015, “Analysis of Using Ferrofluid as an Interface Material in a Field Reversible Thermal Connector,” J. Electron. Package. 137, PP. 21003–21003.

[56] Rank, W. J., Whalen, M. J., 1982, “Apparatus for mounting circuit cards,” U.S. Patent 4 318 157.

[57] Reilly, S., Stubblebine, M., Supowit, J., Catton, I., 2013, “A Novel , Autonomous Thermal Connector,” 29th IEEE Semi-Therm Symposium, Los Angeles, CA.

[58] Chen, H., Solbrekken, G.L., Chen, C., 2016, “Field-Reversible Thermal Connector (RevCon) Challenges : A Review,” IEEE Transaction on Components , Pacaging and Manufacturing Technology, 6, PP. 1181–1197.

[59] Thompson, S.M., Tessler, B.S., Ma, H., Smith, D.E., Sobel, A., 2013, “Ultrahigh thermal conductivity of three-dimensional flat-plate oscillating heat pipes for electromagnetic launcher cooling,” IEEE Trans. Plasma Sci., 41, PP. 1326–1331.

[60] Chang, J.-Y., Prasher, R.S., Prstic, S., Cheng, P., Ma, H.B., 2008, “Evaporative Thermal Performance of Vapor Chambers Under Nonuniform Heating Conditions,” J. Heat Transfer., 130, PP. 121501.

[61] Lee, S.H.K., Chu, S.K., Choi, C.C.C., Jaluria, Y., 2007, “Performance characteristics of vapor chambers with boiling enhanced multi-wick structures,” Annu. IEEE Semicond. Therm. Meas. Manag. Symp., PP. 125–130.

[62] Xie, H., Ali, A., Bhatia, R., 1998, “The use of heat pipes in personal computers,” Therm. Thermomechanical Phenom. Electron. Syst., PP. 442–448.

[63] Peterson, G. P., 1994, An Introduction to Heat Pipes, Wiley, New York.

[64] Khandekar, S., Schneider, M., Schafer, P., Kulenovic, R., Groll, M., 2002, “Thermofluid Dynamic Study of Flat-Plate Closed-Loop Pulsating Heat Pipe,” *Microscale Thermophysical Engineering*, 6, pp. 303-317.

[65] Borgmeyer, B. & H.B. Ma, 2007, “Experimental Investigation of Oscillating Motions in a Flat-Plate Oscillating Heat Pipe,” *Journal of Thermophysics and Heat Transfer,* **21** (2), pp. 405-409.

[66] Xu, G., Liang, S., Vogel, M., 2006, “Thermal Characterization of Pulsating Heat Pipes,” The Tenth Intersociety Conference on Thermal and Thermomechanical Phenomena in Electronics Systems, IEEE, San Diego, U.S.A., pp. 552-556.

[67] Lin, Y.H., Kang, S.W., Wu, T.Y., 2009, “Fabrication of Polydimethylsiloxane (PDMS) Pulsating Heat Pipe” Applied Thermal Engineering, **29** (2-3), pp. 573-580.

[68] Cheng, P., Dong, J., Thompson, S.M., Ma, H.B., 2012, “Heat transfer in the bulk and thin film fluid regions of a rectangular micro groove,” J. Thermophys. Heat Transf., 26, PP. 108–114.

[69] Sha, M.B., Faghri, A., Zhang, Y., 2002, “Analysis of heat transfer in unlooped and looped pulsating heat pipes,” Int. J. of Numerical Methods for Heat and Fluid Flow, 12, PP. 585–609.

[70] Taft, B.S., Williams, A.D., Drolen, B.L., 2012, “Review of Pulsating Heat Pipe Working Fluid Selection,” J. Thermophys. Heat Transf., 26, PP. 651–656.

[71] Mangini, D., Mameli, M., Georgoulas, A., Araneo, L., Filippeschi, S., Marengo, M., 2015, “A pulsating heat pipe for space applications: Ground and microgravity experiments,” Int. J. Therm. Sci., 95, PP. 53–63.

[72] Taft, B.S., Laun, F.F., Smith, S.M., Hengeveld, D.W., 2015, “Microgravity Performance of a Structurally Embedded Oscillating Heat Pipe,” AIAA J. Thermophys. Heat Transf., 29, PP. 329–337.

[73] Van Es, J., Woering, A.A., 2000, “High-acceleration performance of the Flat Swinging Heat Pipe High-acceleration performance of the Flat Swinging Heat Pipe,” SAE Tech. Pap.

[74] Riehl, R.R., 2004, “Characteristics of an open loop pulsating heat pipe,” SAE Tech. Pap. (2004).

[75] Thompson, S.M., Cheng, P., Ma, H.B., 2011, “An experimental investigation of a three-dimensional flat-plate oscillating heat pipe with staggered microchannels,” Int. J. Heat Mass Transf., 54, PP. 3951–3959.

[76] Thompson, S.M., Ma, H.B., Winholtz, R. A., Wilson, C., 2009, “Experimental Investigation of Miniature Three-Dimensional Flat-Plate Oscillating Heat Pipe,” J. Heat Transfer., 131, PP. 43210.

[77] Smoot, C.D., Ma, H.B., 2014, “Experimental Investigation of a Three-Layer Oscillating Heat Pipe,” J. Heat Transfer., 136, PP. 51501.

[78] Borgmeyer, B., Wilson, C., Winholtz, R.A., Ma, H.B., Jacobson, D.L., Hussey, D.S., 2009, "Heat Transport Capability and Fluid Flow Neutron Radiography of Three-Dimensional Oscillating Heat Pipes," Proceedings of the ASME Summer Heat Transfer Conference, ASME, Jacksonville, U.S.A., pp. 371-374.

[79] Taft, B.S., 2013, "Non-Condensable Gases and Oscillating Heat Pipe Operation," Front. Heat Pipes., 4, PP. 13003.

[80] Deckard, C.R., 1989, "Method and Apparatus for Producing Parts by Selective Sintering," U.S. Patent No. 4 863 538.

[81] Murr, L.E., Gaytan, S.M., Medina, F., Lopez, H., Martinez, E., Machado, B.I., Hernandez, D.H., Martinez, L., Lopez, M.I., Wicker, R.B., Bracke, J., 2010, "Next-generation biomedical implants using additive manufacturing of complex, cellular and functional mesh arrays," Philos. Trans. A. Math. Phys. Eng. Sci., 368, PP. 1999–2032.

[82] Tapia, G., Elwany, A., 2014, "A Review on Process Monitoring and Control in Metal-Based Additive Manufacturing," J. Manuf. Sci. Eng., 136, PP. 60801.

[83] Thompson, S.M., Bian, L., Shamsaei, N., Yadollahi, A., 2015, "An overview of Direct Laser Deposition for additive manufacturing; Part I: Transport phenomena, modeling and diagnostics," Addit. Manuf., 8, PP. 36–62.

[84] Shamsaei, N., Yadollahi, A., Bian, L., Thompson, S.M., 2015, "An overview of Direct Laser Deposition for additive manufacturing; Part II: Mechanical behavior, process parameter optimization and control," Addit. Manuf., 8, PP. 12–35.

[85] Bian, L., Thompson, S.M., Shamsaei, N., 2015, "Mechanical Properties and Microstructural Features of Direct Laser-Deposited Ti-6Al-4V," Jom., 67, PP. 629–638.

[86] Sterling, A.J., Torries, B., Shamsaei, N., Thompson, S.M., Seely, D.W., 2016, "Fatigue behavior and failure mechanisms of direct laser deposited Ti-6Al-4V," Mater. Sci. Eng. A., 655, PP. 100–112.

[87] Thompson, S.M., Aspin, Z.S., Shamsaei, N., Elwany, A., Bian, L., 2015, "Additive manufacturing of heat exchangers: A case study on a multi-layered Ti-6Al-4V oscillating heat pipe," Addit. Manuf., 8, PP. 163–174.

[88] Lemmon, E.W., McLinden, M.O., Friend, D.G., "Thermophysical Properties of Fluid Systems," in: P.J. Linstrom, W.G. Mallard (Eds.), NIST Chem. WebBook, NIST Stand. Ref. Database 69, National Institute of Standards and Technolgy, Gaithersburg, n.d.

[89] Rausch, M.H., Kretschmer, L., Will, S., Leipertz, A., Fröba, A.P., 2015, "Density, surface tension, and kinematic viscosity of hydrofluoroethers HFE-7000, HFE-7100, HFE-7200, HFE-7300, and HFE-7500," J. Chem. Eng. Data., 60, PP. 3759–3765.

[90] "3M Thermal Management Fluids: Cool Under Fire - Dielectric heat transfer fluid solutions for military and aerospace applications," (2009).

[91] Faghri, A., Zhang, Y., 2006, "Transport Phenomena in Multiphase System," ElsevierAcademic Press, Burlington.

[92] Faghri, A., Zhang, Y., Howell, J., 2010, "Advanced Heat and Mass Transfer," Global Digital Press, Columbia.

[93] Hao, T., Ma, X., Lan, Z., Li, N., Zhao, Y., Ma, H., 2014, "Effects of hydrophilic surface on heat transfer performance and oscillating motion for an oscillating heat pipe," Int. J. Heat Mass Transf., 72, PP. 50–65.

[94] Rhodes, M.J, Taylor, M.R., Monroe, J.G., Thompson, S.M., 2014, "Experimental Investigation of a Flat-Plate Oscillating Heat Pipe with Modified Evaporator and Condenser," ASME Int. Mech. Eng. Congr. Expo., IMECE2014-39188.

[95] Smoot, C.D., Ma, H.B., 2011, "an Experimental Investigation of Hybrid Oscillating Heat Pipe," Front. Heat Pipes., 2, PP. 1–6.

[96] Santodonato, L., Bilheux, H., Bailey, B., Bilheux, J., Nguyen, P.T., Tremsin, A.S., Selby, D.L., Walker, L., 2015, "The CG-1D neutron imaging beamline at the Oak Ridge National Laboratory High Flux Isotope Reactor," Phys. Procedia., 69, PP. 104–108.

[97] Crow, L., Robertson, L., Bilheux, H., Fleenor, M., Iverson, E., Tong, X., Stoica, D., Lee, W.T., 2011, "The CG1 instrument development test station at the High Flux Isotope Reactor," Nucl. Instruments Methods Phys. Res. A., 634, PP. S71–S74.

[98] Kang, M., Bilheux, H., Voisin, S., Cheng, C., Perfect, E., Horita, J., Warren, J.M., 2013, "Water calibration measurements for neutron radiography: application to water content quantification in porous media," Nucl. Instruments Methods Phys. Res. Sect. A., 708, PP. 24–31.

[99] Zuo, Z.J., North, M.T., Wert, K.L., 2001, "High Heat Flux Heat Pipes for Cooling of Electronics," IEEE Trans. Components Package. Technol., 24, PP. 220–225.

[100] Holley, B., Faghri, A., 2005, "Analysis of pulsating heat pipe with capillary wick and varying channel diameter," Int. J. Heat Mass Transf., 48, PP. 2635–2651.